NASA CONTRACTOR REPORT

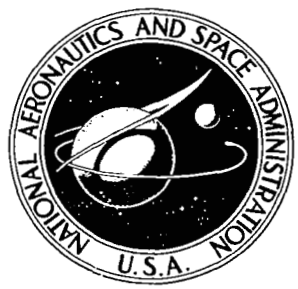

NASA CR-1971

APPLICATION OF ISOTENSOID FLYWHEELS TO SPACECRAFT ENERGY AND ANGULAR MOMENTUM STORAGE

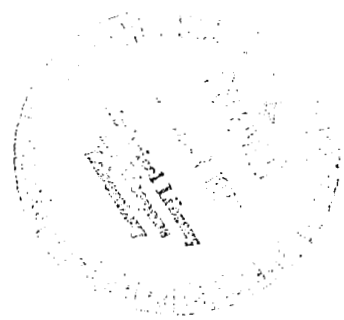

by L. R. Adams

Prepared by
ASTRO RESEARCH CORPORATION
Santa Barbara, Calif. 93103
for

NATIONAL AERONAUTICS AND SPACE ADMINISTRATION • WASHINGTON, D. C. • FEBRUARY 1972

1. Report No.	2. Government Accession No.	3. Recipient's Catalog No.
NASA CR-1971		

4. Title and Subtitle	5. Report Date
APPLICATION OF ISOTENSOID FLYWHEELS TO SPACECRAFT ENERGY AND ANGULAR MOMENTUM STORAGE	February 1972
	6. Performing Organization Code
7. Author(s)	8. Performing Organization Report No.
L. R. Adams	ARC-R-423
	10. Work Unit No.
9. Performing Organization Name and Address	11. Contract or Grant No.
Astro Research Corporation Santa Barbara, California 93103	NAS7-728
	13. Type of Report and Period Covered
12. Sponsoring Agency Name and Address	Contractor Final Report
National Aeronautics and Space Administration Washington, D.C. 20546	14. Sponsoring Agency Code
	RWS

15. Supplementary Notes

16. Abstract

Studies and experiments with concept for expandable flywheel structures using iso-tensoid filament geometry and centrifugal force.

17. Key Words (Suggested by Author(s))	18. Distribution Statement
Iso-tensoids, expandable structures, control moment gyros	Unlimited

19. Security Classif. (of this report)	20. Security Classif. (of this page)	21. No. of Pages	22. Price*
Unclassified	Unclassified	67	$3.00

*For sale by the National Technical Information Service, Springfield, Virginia 22151

SUMMARY

The application of a concept in isotensoid flywheel design to spacecraft energy and angular momentum storage is studied. Systems employing the isotensoid flywheel are evaluated in terms of energy density (watt-hr/lb) and angular momentum density (ft-lb-sec/lb) and compared with standard electrochemical storage devices and rigid control-moment gyro wheels.

Experimentation is reported which was conducted on isotensoid flywheels. Quantitative measurements were taken of: 1) strain in fabric flywheels, 2) packaging the fabric flywheel, and 3) actual energy stored in a steel-cable flywheel.

CONTENTS

TABLES AND ILLUSTRATIONS

ILLUSTRATIONS (CONT'D)

SYMBOLS

A	Constant
d	Depth of discharge
E	Energy
F	Force
f	Number of degrees of freedom
g	Gravitational constant (32.2 ft/sec^2)
H	Angular momentum
h	Height above equator
I	Moment of inertia
k	Radius of gyration
ℓ	Length; length from equator; lifetime
m	Mass
m'	Mass per unit length
N	Number of circles
P	Power, force
R	r/r_0, nondimensional radius
r	Radius
T	Tension, torque
t	Time
V	Volume
W	Weight
W'	Weight per unit length

x	Width of Stodola wheel
x, y, z	Orthogonal coordinates
Z	Centrifugal force
β	Angle of filament to meridian
Γ	$\rho\omega^2 r_0^2/\sigma$, structure parameter
$\gamma \equiv \rho g$	Weight density
Δ	Incremental change
ϵ	Strain
η	Efficiency
θ	Gimbal angle
$\dot{\theta}$	Gimbal precession rate
λ	T/m'g, specific stress
μ	Coefficient of friction
π	3.14159
ρ	Volume density
σ	Stress, surface density
τ	Period of oscillation
ψ	Gimbal angle
ψ_P	Maxwell potential function
Ω	$m' \omega^2 r_0^2/T$, structure parameter
ω	Wheel spin speed

Subscripts:

0	At rim
1	Power penalty
2	Volume penalty
a	At axis
ave	Average
B	Bearing
c	Compression
d	Disturbance
dep	Deployment
disk	Disk
eff	Effective
G	Gimbal
gen	Generator
I	Inter-filament
i	Element number
mast	Mast
min	Minimum
PS	Power system
R	Recoverable
SM	Spin motor
T	Total

TM	Torque motor
t	Tension
ult	Ultimate
vol	Volume
w	Working
wd	With disk
wod	Without disk

INTRODUCTION

References 1 and 2 deal with spinning filamentary structures, with primary attention given to isotensoid versions. The development of a flat (two dimensional) filamentary isotensoid flywheel is reported in Reference 1; the development of a generalized three-dimensional concept of this flywheel is covered in Reference 2. The application of these structures to spacecraft energy and angular momentum storage is the subject of this study.

A special case was chosen from the general solutions given in References 1 and 2, which has relative simplicity in mathematical form and physical shape. The merits of energy and angular momentum storage systems which use this flywheel are evaluated by comparison with the conventional methods which involve electrochemical storage batteries and rigid control-moment gyro wheels. Full advantage is taken of filament strength, which yields high energy and momentum densities; and of deployability, which reduces rotation rates and increases momentum density.

Other types of flywheels are discussed and compared with the isotensoid flywheel on the basis of energy and angular momentum densities.

THE ISOTENSOID FILAMENTARY FLYWHEEL

In Reference 1, Kyser develops a system of equations which describes isotensoid filamentary disks. An infinite number of solutions describing fiber patterns is possible. One pattern is of special interest; each fiber follows a circular path, the diameter of each circle being equal to the radius of the wheel. The circles pass through the center of the wheel, and are equally spaced in the circumferential direction. This pattern is illustrated in Figure 1.

A more general three-dimensional configuration of isotensoid flywheel is described by Fraser in Reference 2. Here each fiber path is helical instead of circular. The configuration is illustrated in Figure 2. The specialized disk shape is formed from this three-dimensional flywheel by reducing the helix height to zero.

Geometrical Properties

The isotensoid flywheel considered herein is described by the following set of equations:

$$\sin\beta = \sqrt{\frac{\Omega}{2}}\, R \tag{1}$$

$$h = r_0 \sqrt{(1 - \Omega/2)/(\Omega/2)}\,(\pi/2 - \sin^{-1} R) \tag{2}$$

where

$$\Omega = \frac{m' \omega^2 r_0^2}{T} \tag{3}$$

is a "structure" parameter by which the shape is controlled. Unit definitions, taken from Reference 2, are:

m' is the mass per unit fiber length

ω is the spin speed

r_0 is the flywheel radius

T is the fiber tension

β is the fiber angle to the meridian

$R = r/r_0$ is the nondimensional radial distance

h is the height above the equator

Derived relations are:

$$\ell = r_0(\pi/2 - \sin^{-1} R)/\sqrt{\Omega/2} \tag{4}$$

and

$$\cos\alpha = \sqrt{(1 - \Omega/2)/(1 - \Omega R^2/2)} \tag{5}$$

where ℓ is the fiber distance from the equator and α is the meridian angle to the spin axis.

The helix angle, β_0, is obtained from Equation (1) with $R = 1$,

$$\beta_0 = \sin^{-1}\sqrt{\frac{\Omega}{2}} \tag{6}$$

The distance between the two points at which the system of helices intersects the axis (the "hub separation") is determined from Equation (2) with $R = 0$,

$$2\,h_a = \pi\, r_0 \sqrt{(1 - \Omega/2)/\Omega/2)} \tag{7}$$

A continuum of fiber patterns is formed for $0 < \Omega \leq 2$; at $\Omega = 2$ the flat disk results.

Distance between intersections. - The distance, $\Delta\ell$, between adjacent intersections is constant and is equal to

$$\Delta\ell = \frac{\pi\, r_0}{N \sin\beta_0} \tag{8}$$

where N is the number of fiber circles. This property aids in the construction process in that it allows that pattern to be assembled on convenient base boards such as a flat surface, making a square array as in Figure 3. Figures 1 and 3 represent the same object, with the letters A to F indicating corresponding points of intersection. Construction is also possible on a drum formed by connecting points A, E, and F on opposite ends of the array in Figure 3.

Radius of gyration. - For convenience, the circular fiber shape of the disk form is assumed here, but the result also applies to the helical shape. The radius of gyration, k , is derived from the equation

$$k^2 = \frac{\int_\ell r^2\, d\ell}{\ell} , \tag{9}$$

where r and $d\ell$ are as defined in Figure 4, and ℓ is the circumference of the circle. The elemental distance is $d\ell = \frac{1}{2}\, r_0\, d\theta$, and by the cosine law, $r^2 = \frac{1}{2}\, r_0^{\,2}\, (1 - \cos\theta)$. Thus the radius of gyration is

$$k = \sqrt{\frac{1}{2}}\, r_0 . \tag{10}$$

Physical Properties

Tension. - The tension throughout the network is, from Equation (3),

$$T = \frac{m' r_0^2 \omega^2}{\Omega} \tag{11}$$

Energy density. - The rotational kinetic energy of the wheel is $E = 1/2\ m\ k^2\ \omega^2$, or by Equations (10) and (11), $E/m = \Omega T/4m'$. The quantity, $T/m'g$, is defined as the specific stress, λ , of the fiber. The energy density realized at the specific working stress is

$$\frac{E}{m} = \frac{\Omega}{4}\ g\ \lambda_w \tag{12}$$

A general statement is derived in Appendix A relating the energy density of an isotensoid flywheel to its specific working stress, λ_w . The energy density of an isotensoid disk ($\Omega = 2$) is, by Equation (A-2), considering that there is one degree of freedom for stress action, $E/m = 1/2\ g\ \lambda_w$. Compare to Equation (12).

Momentum density. - The angular momentum density of a wheel is $H/m = k^2\ \omega$, or in terms of energy density

$$\frac{H}{m} = k \sqrt{2\ \frac{E}{m}} \tag{13}$$

$$\frac{H}{m} = r_0 \sqrt{\frac{\Omega}{4}\ g\ \lambda_w} \tag{14}$$

Energy storage and recovery by momentum exchange. - For storage of electrical energy, power from solar cells would drive the flywheel spin motor, thus increasing the kinetic energy of the flywheel. Energy is recovered through generator action. Accompanying this energy exchange is an angular momentum exchange

which, if undesirable, may be alleviated by rotating a pair of flywheels in opposite directions.

This method of energy exchange necessitates the use of variable speed electric motors. Such motors are not equally efficient at all speeds; a maximum-minimum speed ratio of three, at the present state of development, gives a good trade-off between flywheel utilization and motor efficiency (Ref. 3). Since the flywheel energy is proportional to the rotation speed squared, 1/9 of the energy is not recoverable. Then the recoverable energy density of the isotensoid flywheel is

$$\left(\frac{E}{m}\right)_R = \frac{8\Omega}{36} g \lambda_w \qquad (15)$$

Energy storage and recovery by hub distance variation. - The spindle-shaped flywheel, consisting of helical fibers which extend from one hub to another, was introduced on page 6. Varying the distance between the hubs changes the moment of inertia of the flywheel. If constant angular momentum is assumed, the resulting change in rotational energy of the flywheel must reflect an equal but opposite change in potential energy caused by forcing the hubs to move through a distance.

In Figure 5, power from the solar cells drives the motor-driven pump which moves fluid into the chamber between the hubs, forcing them apart. Allowing the hubs to move toward each other forces the fluid through the turbine generator and recovers the stored energy. There is no exchange of angular momentum in this process.

The energy stored in the system is equal to the difference between the kinetic energy of the wheel in that state and at the ground (disk) state. The kinetic energy is (from Eq. (12)):

$$E = \frac{\Omega}{4} mg \lambda_w$$

In the disk configuration Ω is 2; thus the energy stored is

$$\Delta E = \frac{\Omega}{4} mg \lambda_w - \frac{1}{2} mg \lambda_{disk} \tag{16}$$

where λ_{disk} is the specific stress in the disk form.

With this method, no angular momentum is exchanged. The angular momentum is constant and equal to that in the disk form. By Equation (14),

$$r_0 \sqrt{\Omega \lambda_w} = r_{0_{disk}} \sqrt{2\lambda_{disk}} \tag{17}$$

Combining Equations (16) and (17) yields the stored energy in terms of Ω, r_0, and λ_w:

$$\Delta E = \frac{\Omega}{4} mg \lambda_w \left[1 - \left(\frac{r_0}{r_{0_{disk}}} \right)^2 \right] \tag{18}$$

The fiber length between hubs is, of course, constant; this distance is, from Equation (4),

$$\ell = \frac{\pi r_0}{\sqrt{\frac{\Omega}{2}}} = \pi r_{0_{disk}}' .$$

Then the structure parameter is

$$\Omega = 2 \left(\frac{r_0}{r_{0_{disk}}} \right)^2 . \tag{19}$$

Combining Equations (18) and (19) yields

$$\frac{\Delta E}{m} = \frac{1}{2} g \lambda_w \left[\left(\frac{r_0}{r_{0_{disk}}} \right)^2 - \left(\frac{r_0}{r_{0_{disk}}} \right)^4 \right],$$

which maximizes for $r/r_{0_{disk}} = \sqrt{1/2}$, at a value of

$$\left(\frac{\Delta E}{m} \right)_{max} = \frac{1}{8} g \lambda_w \qquad (20)$$

Thus the recoverable energy by this method is 28% of the energy stored by the variable-momentum flywheel.

Interfiber force. - The force exerted by one fiber on an intersecting fiber is (Ref. 2)

$$F_I = \frac{\Omega R T \operatorname{ctn}\beta \sin\alpha}{r_0} \Delta\ell .$$

Inserting β , α , and $\Delta\ell$ from Equation (1), (5), and (8) yields

$$F_I = \frac{\sqrt{2\Omega}\, \pi T}{N} \sqrt{1 - R^2} \qquad (21)$$

Methods of Construction

Joints. - The interfiber force discussed above is provided at the intersections, with various types of joints being possible, including: 1) weaving, where the interfiber force is supplied by friction; 2) knots or mechanical joints; and 3) glue.

Fabric wheel. - Fabric wheels may be woven, knotted, or glued; knotting is the least satisfactory, in that knot placement

is critical. A disk and a spindle-shaped wheel, both constructed by weaving Dacron tape, are shown in Figures 6 and 7.

Steel cable wheel. - A flywheel consisting of a set of circular cables can be constructed as shown in Figure 8, with the intersections held by swaged copper tubes.

Semi-solid flywheel. - The circular fiber disk flywheel shown in Figure 1 may be constructed using solid links instead of flexible fibers between the intersections. Each arc between adjacent intersections is replaced by the corresponding chord, as in Figure 9. Each link is hinged freely at the joints. The packing of this wheel is demonstrated in Figure 10.

Rim mass. - It may be necessary or desirable to alter the shape of an isotensoid flywheel for practical reasons. For instance, the fabric disk shown in Figure 6 has a truncated circular pattern; for operation a rim mass must be added to give the isotensoid property. The mass required is that which provides a centrifugal force equal to that which is present at the same radial distance in an untruncated flywheel.

OTHER TYPES OF FLYWHEELS

The Stodola Wheel

A constant biaxial stress wheel was developed by Stodola (Ref. 4). Since two dimensions of stress are utilized, it is expected from the Maxwell relation (App. A) that the ultimate energy density of the Stodola wheel should be $g\,\lambda_w$.

The shape of Stodola's wheel is given as

$$x = x_a\, e^{-\frac{1}{2}\Gamma\, R^2} , \tag{22}$$

where x is the width of the wheel at a radius $R = r/r_0$, as in Figure 11; and Γ is a structure parameter, defined by $\Gamma = \rho\, \omega^2\, r_0{}^2/\sigma$. In practice the wheel is truncated arbitrarily at $R = 1$; this results in a near-ideal flywheel if Γ is large, while for small Γ the flywheel approaches a flat disk.

Energy density. - The radius of gyration of this body is

$$k = r_0 \sqrt{\frac{2}{\Gamma} - \frac{1}{e^{\frac{1}{2}\Gamma} - 1}} . \tag{23}$$

Its energy density is thus

$$\frac{E}{m} = \left(1 - \frac{1}{2}\, \frac{\Gamma}{e^{\frac{1}{2}\Gamma} - 1}\right) g\, \lambda_w \tag{24}$$

For large Γ , the second term in the parentheses is small. Thus the energy density does approach $g\,\lambda_w$ in the ideal case of large Γ .

Momentum density. - The momentum density of the Stodola wheel is

$$\frac{H}{m} = r_0 \left(\frac{2}{\sqrt{\Gamma}} - \frac{\sqrt{\Gamma}}{e^{\frac{1}{2}\Gamma} - 1} \right) \sqrt{g \lambda_w} \qquad (25)$$

This function is plotted in Figure 12, along with Equation (24). It is seen that the momentum density maximizes at $\Gamma \simeq 5$, with $(H/m)_{max} \simeq \sqrt{1/2\ g\ \lambda_w}$.

Standard Flywheels

The energy density, momentum density, and rotation speed of various types of flywheels are given in Table I. Table II lists the specific working stress of typical flywheel materials.

FLYWHEEL APPLICATION TO SPACECRAFT ENERGY STORAGE

In spacecraft in which the primary source of power is the sun through solar cells there are two fundamental difficulties. Loss of power occurs when the spacecraft enters the shadow of a moon or planet, and peak load power requirements may be higher than solar cell capabilities. Both problems must be solved by energy storage. The method widely used today is the electrochemical storage battery. Types of batteries in use and an analysis of present-day battery storage systems in terms of total energy stored per pound battery weight over the life of the system are given in Appendix B.

The purpose of this section is to examine the efficiency of the flywheel system as a competitive energy-storage device. Only the disk flywheel will be considered here.

The theoretical recoverable energy of the disk is given, by Equation (15) with $\Omega = 2$. The practical recoverable electrical energy must take into account the generator efficiency, η. Thus

$$E_R = \frac{4}{9} m_{disk} g \lambda_w \eta \qquad (25)$$

where m_{disk} is the mass of the disk. The recoverable energy density, considering the masses of the disk, the hub (m_{hub}), the spin motor (m_{SM}), the generator (m_{gen}), the deployment hardware (m_{dep}), and a penalty for package volume (m_{vol}) is

$$\frac{E_R}{m} = \frac{E_R}{m_{disk} + m_{hub} + m_{SM} + m_{gen} + m_{dep} + m_{vol}},$$

or

$$\frac{E_R}{m} = \left[\frac{m_{disk}}{E_R} + \frac{m_{hub}}{E_R} + \frac{m_{SM}}{E_R} + \frac{m_{gen}}{E_R} + \frac{m_{dep}}{E_R} + \frac{m_{vol}}{E_R}\right]^{-1}. \qquad (26)$$

The quantities within the parentheses are as follows:

$\underline{m_{disk}/E_r}$. - By Equation (25), this ratio is $(4/9\ g\ \lambda_w\ \eta)^{-1}$. For this study the disk material is assumed to be stainless steel cable (7 x 7, 1/16-in. diam.), the properties of which are shown in Table II. Then

$$\frac{m_{disk}}{E_R} = \frac{1}{10\ \eta}\ \text{lb/watt-hr} \quad . \tag{27}$$

$\underline{m_{hub}/E_R}$. - Let the mass of the hub be 5% of the disk mass: $m_{hub} = 0.05\ m_{disk}$. By Equation (27), $m_{hub} = 0.05\ E_R/10\eta$. Then

$$\frac{m_{hub}}{E_R} = \frac{0.005}{\eta} \tag{28}$$

$\underline{m_{SM}/E_R\ ;\ m_{gen}/E_R}$. - These quantities are dependent on spacecraft power requirements. Let P_{ave} be the average power consumed, and the peak power demand be $4\ P_{ave}$. The orbital period is 1.5 hours and the spacecraft is in shadow for 0.5 hour. During darkness, power is provided solely by the flywheel so that $E_R = 1/2\ P_{ave}$. The solar cells must supply a power equal to $(1 + 1/2\eta)\ P_{ave}$, to supply P_{ave} to the spacecraft during the lighted period and $1/2\ P_{ave}$ to the flywheel through a spin motor of efficiency, η , (assumed herein to be the same as the generator efficiency). The spin motor power must be sized so that its output power may vary from zero to $3/2\ P_{ave}$. The generator must be sized so that its output power may vary from zero to $4\ P_{ave}$ (see Fig. 13).

Survey data on weights, powers, and efficiencies of variable-speed d.c. motors and generators show that the weight, m , in pounds is approximately $1.25\sqrt{P}$, where P is the output power in watts. The efficiency of each varies with output power level, with an average value of about 60%.

The spin motor mass is then $m_{SM} = 1.25\sqrt{3/2\ P_{ave}} = 1.25\sqrt{3E_R}$,

or
$$\frac{m_{SM}}{E_R} = \frac{2.17}{\sqrt{E_R}} \quad . \tag{29}$$

The generator mass is $m_{gen} = 1.25\sqrt{4P_{ave}} = 1.25\sqrt{8E_R}$, or

$$\frac{m_{gen}}{E_R} = \frac{3.53}{\sqrt{E_R}} \tag{30}$$

$\underline{m_{dep}/E_R}$. - The deployment canister could be similar to that shown in Figure 14. The surface area of the cylinder is $A = 4\pi(0.11\ r_{disk})^2$, or $A = 0.33\ E_R$ square feet. A penalty of 0.1 lb/ft^2 gives a mass $m_{dep} = 0.033\ E_R$ for the deployment hardware, or

$$\frac{m_{dep}}{E_R} = 0.033 \tag{31}$$

$\underline{m_{vol}/E_R}$. - The deployment package volume is that of a sphere of radius $0.03\ r_{disk}$: $V = 4/3\ \pi(0.03\ r_{disk})^3$, or $V = 1.25 \times 10^{-5}\ E_R^{3/2}$.

A penalty of 1.0 lb/ft^3 is assumed, so that

$$\frac{m_{vol}}{E_R} = 1.25 \times 10^{-5}\sqrt{E_R} \tag{32}$$

The recoverable energy of the system is obtained by inserting Equations (27), (28), (29), (30), (31), and (32) into Equation (26), with $\eta = 0.6$:

$$\frac{E_R}{m} = \left[0.21 + \frac{5.7}{\sqrt{E_R}} + 1.25 \times 10^{-5} \sqrt{E_R}\right]^{-1} \qquad (33)$$

Equation (33) is plotted in Figure 15, over a range of 10 watt-hr $\leq E_R \leq$ 10 000 watt-hr . At E_R = 240 watt-hr, the energy density of the system equals that of a nickel-cadmium battery energy storage system (see Appendix B). For E_R > 240 watt-hr, the flywheel system is superior; at $E_R \cong$ 500 000 watt-hr, the function is maximum, with E_R/m = 4.41 watt-hr/lb.

Thus for spacecraft in near-earth orbit in which the average power requirement is less than 500 watts the Ni-Cd battery energy storage system is better; for P_{ave} > 500 watts the flywheel system provides higher energy density.

FLYWHEEL APPLICATION TO SPACECRAFT ATTITUDE CONTROL

Common means of attitude control in spacecraft include gas jets, reaction wheels, and control-moment gyros (CMG). Gas jets are located at the periphery and torque the spacecraft by expelling gas. Reaction wheels employ a fixed-axis rotor with control torques obtained by motor torquing of the rotor. Control of a disturbance torque, T_d, on the rotor spin axis is obtained by accelerating the rotor according to $\dot{\omega} = T_d/I_w$, where ω is the rotor speed and I_w is the wheel moment of inertia.

A CMG employs a movable-axis rotor. Precession of the rotor causes a torque to be exerted on the vehicle perpendicular to both the spin and the precession axes. Referring to Figure 16, for control of a disturbance torque, T_d, about the y-axis the rotor gimbals are precessed at the rate, $\dot{\theta} = -T_d/H \cos\theta$, about the z-axis. It is seen that at $\theta = \pi/2$ "gimbal lock" occurs; i.e., no torque can be generated about the rotor spin axis. For maneuvering the vehicle, a slew rate of $\dot{\psi} = H\Delta(\sin\theta)/I_y$ about the y-axis is possible by precessing the rotor about the z-axis to effect a change in $\sin\theta$. The vehicle continues to rotate until the rotor is returned to the original position.

Large, high-momentum-density flywheels have definite advantages for all of these momentum exchange devices. In the case of the CMG, a high-momentum density increases the available control momentum, reduces the required gimbal precession rate, and increases the maneuvering capability (all per pound of flywheel weight). For the reaction wheel, a large wheel reduces the required rotor acceleration for a given disturbance torque thereby prolonging the time to wheel stall speed.

External Isotensoid Flywheel CMG

A CMG can be constructed using a large external isotensoid flywheel as a basic unit. The system considered is pictured in Figure 17. The flywheel is mounted on the end of a deployable boom and rotates in the void. Precession is possible about two axes.

A standard CMG has a solid rotor rotating in an enclosure containing gas at low pressure (Ref. 5). Windage drag is considerable, and the limited size of the system restricts the wheel angular momentum. An analysis optimizing the standard CMG by parameterizing rotor angular momentum and torque magnitude is summarized (from Ref. 5) in Appendix C. The external-wheel CMG is evaluated by comparing it with the optimized standard system. The basis of comparison is the ratio of wheel angular momentum to system launch weight, at various torque requirements.

The weights of the major components of the external wheel CMG are calculated as follows:

Flywheel. - The weight of the flywheel is determined from its size and specific working stress. Its momentum density (Eq. (14), with $\Omega = 2$), is

$$\frac{H}{m} = r_0 \sqrt{\frac{1}{2} g \lambda_w} , \tag{34}$$

and the mass of the wheel is related to its average surface density, σ , by

$$m = \sigma \pi r_0^2 . \tag{35}$$

The weight of the flywheel is $W_{disk} = mg$, or

$$W_{disk} = \left(\frac{2\sigma \pi g^2}{\lambda_w} \right)^{1/3} H^{2/3} \tag{36}$$

Gimbals. - The weight of the gimbals is assumed proportional to the weight of the flywheel:

$$W_G = (\text{Const})\ W_{disk} . \tag{37}$$

For the purpose of this study the constant is assumed, conservatively, to be unity.

Boom. - The boom may be an Astromast beam of the coilable lattice type. This mast is automatically deployable, and its weight per unit length (Ref. 6, Eq. (B-5); $f = 4.14$, $\rho = 0.070$ pci , $C_I = C_A = 1$, $p = 0.85$, $SF_Y = 10^5$) is

$$W' = 1.45 \times 10^{-2} \, T^{2/3}$$

where W' is in pounds/foot and T is the bending moment in ft-lb. The length of the mast should be at least as large as the wheel radius so that the wheel can be precessed. If the mast is assumed to be 10% larger, the mast weight is

$$W_{mast} = 1.6 \times 10^{-2} \, r_0 \, T^{2/3}$$

The wheel radius, by Equations (34) and (35) is

$$r_0 = \left(\frac{H}{\sqrt{\frac{1}{2} g \lambda_w \sigma \pi}} \right)^{1/3} . \qquad (38)$$

The weight of the mast is then

$$W_{mast} = 0.016 \left(\frac{H}{\sqrt{\frac{1}{2} g \lambda_w \sigma \pi}} \right)^{1/3} T^{2/3}$$

This weight is increased by 50% to include the deployment canister and associated hardware. Then the weight of the boom is

$$W_B = 0.024 \left(\sqrt{\frac{1}{2} g \lambda_w \sigma \pi} \right)^{-1/3} H^{1/3} \, T^{2/3} \qquad (39)$$

Torque motors. - The weight of the torque motors is determined by using the same relations as in the standard CMG:

$$W_{TM} = 1.76 \times 10^{-3} \left(\frac{T^2}{H}\right)^{1.77} \tag{40}$$

Spin motor. - In the standard CMG, the weight of the spin motor is $W_{SM} = 1.5 + P_B/24$; windage loss terms are neglected. P_B is the bearing power loss in watts, and is $P_B = \mu T_{ave}\, r_B\, \omega/\ell$, where μ is the coefficient of bearing fraction, T_{ave} is the average torque, r_B is the shaft radius at the bearing, ω is the spin speed, and ℓ is the distance from flywheel to bearing. If it is assumed that $\mu = 0.01$, $T_{ave} = 0.1\ T$, and $r_B/\ell = 0.1$, the weight of the spin motor is

$$W_{SM} = 1.5 + \frac{10^{-4}\ \omega}{24}\ T \ . \tag{41}$$

The spin speed is (Table I)

$$\omega = \frac{1}{r_0}\sqrt{2g\ \lambda_w} \ . \tag{42}$$

Then the weight of the spin motor is (Eqs. (41), (42), and (38))

$$W_{SM} = 1.5 + 8.3 \times 10^{-6} \left[\left(\frac{1}{2}\ g\ \lambda_w\right)^2\ \sigma\ \pi\right]^{1/3} \frac{T}{H^{1/3}} \tag{43}$$

Power system. - The weight of the power system is

$$W_{PS} = A_1\ P \tag{44}$$

where A_1 is a constant arbitrarily set at 1.0 lb/watt (as in the standard CMG) and P is the sum of the spin and torque motor powers. The spin-motor power is $P_{SM} = P_B/0.60$, or

$$P_{SM} = 3.3 \times 10^{-4} \left[\left(\frac{1}{2} g \lambda\right)^2 \sigma \pi\right]^{1/3} \frac{T}{H^{1/3}} . \quad (45)$$

The average torque motor power is

$$P_{TM_{ave}} = 0.03 \frac{T^2}{H} , \quad (46)$$

as in the standard CMG.

The total power, P, is the sum of Equation (45) and twice Equation (46)(there are two torque motors), so that the weight of the power system is, from Equation (44),

$$W_{PS} = 3.3 \times 10^{-4} \left[\left(\frac{1}{2} g \lambda_w\right)^2 \sigma \pi\right]^{1/3} \frac{T}{H^{1/3}} + 0.06 \frac{T^2}{H} \quad (47)$$

Volume. - The volume of the packaged CMG is assumed to be the volume of a sphere having a radius 1/5 that of the deployed flywheel:

$$V = \frac{4}{3} \pi (0.2 r_0)^3 . \quad (48)$$

This volume is penalized in the same manner as the power supply, in this case with a factor of 1.0 lb/cu ft. Then by Equations (48) and (38), the weight due to the volume of the system is

$$W_{vol} = \frac{0.034}{\sqrt{\frac{1}{2} g \lambda_w \sigma \pi}} H . \qquad (49)$$

Total weight. - The weight of the entire assembly is the sum of Equations (36), (37), (39), (40), (43), (47), and (49):

$$W_T = 2\left(\frac{2\sigma \pi g^2}{\lambda_w}\right)^{1/3} H^{2/3}$$

$$+ 0.024 \left(\sqrt{\frac{1}{2} g \lambda_w \sigma \pi}\right)^{-1/3} H^{1/3} T^{2/3}$$

$$+ 0.00176 \left(\frac{T^2}{H}\right)^{1.77}$$

$$+ 1.5 + 8.3 \times 10^{-6} \left[\left(\frac{1}{2} g \lambda_w\right)^2 \sigma \pi\right]^{1/3} \frac{T}{H^{1/3}}$$

$$+ 3.3 \times 10^{-4} \left[\left(\frac{1}{2} g \lambda_w\right)^2 \sigma \pi\right]^{1/3} \frac{T}{H^{1/3}} + 0.06 \frac{T^2}{H}$$

$$+ \frac{0.034}{\sqrt{\frac{1}{2} g \lambda_w \sigma \pi}} H . \qquad (50)$$

Specific Example of External-Wheel CMG

Equation (50) will now be evaluated for a specific model isotensoid flywheel. The material is 1/16-in. 7 x 7 stainless steel cable. The breaking strength determined experimentally is 900 lb, and the linear density is 0.0075 lb/ft. Then the specific working stress is $\lambda_w = 1/2\ \lambda_{ult} = 60\ 000$ ft. Assume that the

net is designed so that the average surface density is $\sigma_g = 0.075$ lb/ft^2 . Then Equation (50) becomes

$$W_T = 0.126\ H^{2/3} + 0.0125\ H^{1/3}\ T^{2/3} + 0.00176\left(\frac{T^2}{H}\right)^{1.77}$$

$$+ 1.5 + 0.639\ \frac{T}{H^{1/3}} + 0.06\ \frac{T^2}{H} + 0.0045\ H \qquad (51)$$

The quantity, H/W_T, is the total control capacity per pound CMG, which is to be compared with that of the standard CMG.

$$\frac{H}{W_T} = \left[0.126\ H^{-1/3} + 0.0125\left(\frac{T}{H}\right)^{2/3} + 0.00176\ \frac{T^{3.54}}{H^{2.77}}\right.$$

$$\left. + \frac{1.5}{H} + 0.639\ \frac{T}{H^{4/3}} + 0.06\left(\frac{T}{H}\right)^2 + 0.0045\right]^{-1} \qquad (52)$$

This quantity is plotted in Figure 18, using Equation (52) and data reported in Appendix C for the standard CMG, for comparison. Itemized weights and other parameters are listed in Table III, comparing the two systems.

The results of this analysis, summarized in Figure 18, indicate that the external-flywheel CMG is superior to the standard CMG in total control capability per pound of system weight. At comparable rotor momenta, the external wheel model has only one-fourth the weight of the standard model. The standard CMG is restricted to angular momenta up to about 2000 ft-lb-sec; the external wheel model is not so limited and may thus attain control densities (H/W_T) an order of magnitude higher than that possible with the standard CMG. In addition, the external-wheel CMG provides higher control torques because of its large angular momentum.

EXPERIMENTATION

Test Articles and Methods

The following types of flywheels were constructed: 1) woven Dacron tape isotensoid disk flywheel with rim mass, 2) woven Dacron tape isotensoid spindle flywheel, and 3) steel cable isotensoid disk flywheel. Models were spun in an evacuated spin chamber up to speeds of 15 000 rpm.

Dacron disk. - The disk was fabricated on a drum, similar to that shown in Figure 19, except that only half the drum was used (tapes turned 90° at center of drum, so that only one set of nails was used). Upon removal from the drum the disk was put on a ring, as shown in Figure 6, and spun in the spin chamber.

The Dacron tape had a breaking strength of 145 lb and a linear density of 1.05×10^{-3} lb/ft, so that its specific working stress (at half ultimate) was $\lambda_w = 69\ 000$ ft . Its energy density at this stress level is

$$\frac{E}{m} = 12.6 \text{ watt-hr/lb} .$$

Its modulus of elasticity was measured to be

$$\frac{\Delta \ell / \ell}{T} = 0.00069 \text{ lb}^{-1} . \tag{53}$$

The disk had a radius of $r_0 = 0.77$ ft, and since $\Omega = 2$ in the disk form, Equation (11) gives the tension in the disk to be

$$T = 10^{-5} \omega^2 . \tag{54}$$

Since the fabric is in constant tension, strain is uniform over the disk, and the expansion of the radius is predicted by Equations (53) and (54):

$$\frac{\Delta r_0}{r_0} = 6.9 \times 10^{-9} \omega^2 \qquad (55)$$

The disk was observed, using a strobe light, for changes in radius under variations in rotation speed.

Attempts were made to package the disk by squeezing the material into the space inside the inner ring, and estimates of packaged volume were made.

Dacron spindle. - The spindle shaped (double-hub) model wheel was constructed of the same material as the Dacron disk, using the full drum for fabrication, as shown in Figure 19. It had a smaller radius (r_0 = 0.62 ft). Due to its shape, its structure parameter was Ω = 1.83. Therefore its energy density at a specific working stress of half ultimate is (Eq. (12)).

$$\frac{E}{m} = 11.5 \text{ watt-hr/lb} .$$

Its theoretical radial elongation is

$$\frac{\Delta r_0}{r_0} = 4.2 \times 10^{-9} \omega^2 \qquad (56)$$

Steel cable. - The steel cable disk flywheel was constructed of 7 x 7 stainless steel cable, 1/16 in. diameter. The disk was composed of 20 individual cable circles each 27 in. long, with single-shank balls swaged on the ends. A 3.00 in. diameter hub was constructed to hold the ends, and the pattern was held by swaging copper tubes at the intersections, each 1.50 in. apart.

Swaging was done with a special tool which ensured that proper angles and lengths existed at and between the intersections. The finished flywheel and its associated construction equipment are shown in Figure 8.

The cable had a measured breaking strength of 900 lb and a linear density of 6.25×10^{-4} lb/in. Its specific working stress (at half ultimate) was $\lambda_w = 60\ 000$ ft, so that its energy density at this stress is

$$\frac{E}{m} = 11.0 \text{ watt-hr/lb} .$$

The model was spun in the evacuated spin chamber, and tests were made to determine experimentally the kinetic energy of the cable flywheel. The kinetic energy of the system (with disk) including the flywheel, shaft, and motor armature is

$$E_{wd} = \frac{1}{2} \left(I_{disk} + I_{shaft} + I_{arm}\right) \omega^2 , \tag{57}$$

which is dissipated by the shaft bearings when the motor power is turned off. The time, Δt_{wd} , for the assembly to stop completely is determined from

$$T\ \bar{\omega}\ \Delta\ t_{wd} = E_{wd} \tag{58}$$

where $\bar{\omega}$ is the average shaft speed during slow-down and T is the bearing drag torque. When the disk is removed, the kinetic energy of the shaft (without disk) is

$$E_{wod} = \frac{1}{2} \left(I_{shaft} + I_{arm}\right) \omega^2 \tag{59}$$

which is dissipated by

$$T\ \bar{\omega}\ \Delta\ t_{wod} = E_{wod} \tag{60}$$

Combination of Equations (57) through (60) gives

$$\frac{\Delta t_{wd}}{\Delta t_{wod}} = \frac{I_{disk} + I_{shaft} + I_{arm}}{I_{shaft} + I_{arm}} + 1 . \qquad (61)$$

The time, Δt_{wd}, for the shaft to stop with the disk in place, and the time, Δt_{wod}, for only the shaft and armature to stop were measured. I_{disk} and I_{shaft} were calculated from their known shapes, and I_{arm} was calculated experimentally (comparing rotational oscillation frequency with that of a standard disk, using a torsion spring, by the formula $\tau_{arm}/\tau_{standard} = \sqrt{I_{arm}/I_{standard}}$). Substituting these quantities into Equation (57) verified the assumed energy of the flywheel.

Test Results

Dacron flywheels. - The woven Dacron disk and spindle flywheels were tested for radial expansion; the results for the disk were compared with Equation (55) and those for the spindle were compared with Equation (56). These results are shown in Figure 20, on which both experimental and theoretical expansions are plotted against spin speed.

Packing experiments with the Dacron disk flywheel indicate that it can be packed into a space within the inner ring. The radius of the inner ring was 20% of the radius of the Dacron flywheel. The volume of the packaged disk was that of a sphere having a radius equal to 15% of the disk radius.

Steel cable flywheel. - Data collected in reference to Equation (61) were:

$\frac{\Delta t_{wd}}{\Delta t_{wod}}$ = 9.8 for initial spin speeds from 100 rps to 200 rps

I_{disk} = 0.0039 slug ft^2 (calculated from geometry)

$$I_{shaft} = 0.000093 \text{ slug-ft}^2 \text{ (calculated from geometry)}$$

I_{arm}, the moment of inertia of the motor armature, was measured by comparing its natural oscillation frequency with that of a standard, using the same torsion spring on both to provide the restoring force. The periods of oscillation, τ, are related to the moments of inertia by

$$\frac{\tau_{arm}}{\tau_{standard}} = \sqrt{\frac{I_{arm}}{I_{standard}}}$$

The shaft (above) was used as the standard. Its natural period was 0.5 sec; the natural period of the armature was 1 sec. Thus $I_{arm} = 4\ I_{disk}$, or

$$I_{arm} = 0.00037 \text{ slug-ft}^2 .$$

Substitution into Equation (61) gives

$$\frac{\Delta t_{wd}}{\Delta t_{wod}} = \frac{0.0039 + 0.000093 + 0.00037}{0.000093 + 0.00037} + 1$$

$$= 10.4$$

which compares favorably with the 9.8 value obtained experimentally from slow-down times.

Discussion of Test Results

The radial expansion tests on the Dacron flywheels were partially successful. In the region of testing, spin speeds were not high enough to cause sufficient strain in the fabric for full comparison with theory, but some expansion was observed.

Although the disk expanded less and the spindle expanded more than theory predicted, both generally followed Equations (55) and (56) (See Fig. 20).

Packing experiments indicate that the filamentary flywheel could be packed into a sphere having a radius 15% of the flywheel radius (possibly less if a less dense material than woven Dacron is used in the flywheel).

The cable flywheel exercise, in which its energy was calculated both geometrically and through power dissipation, proved successful. The flywheel, with about 15% of the mass of the system, held 89% of the energy.

CONCLUSIONS AND RECOMMENDATIONS

The analyses and experimentation described herein indicate that the isotensoid filamentary flywheel could function very well as an energy or angular-momentum storing device.

In energy storage, the isotensoid flywheel has shown that it is superior to the nickel-cadmium battery in systems of average power greater than 500 watts. In systems above 10 kw, it has more than twice the energy density of the Ni-Cd battery. Power surges would not have an adverse effect on the flywheel as they do on the Ni-Cd battery.

In control-moment gyroscope applications, the large external isotensoid flywheel appears to be far superior to the standard CMG. A characteristic of the flexible wheel which deserves further attention is dynamic deformation of the wheel. The CMG is essentially a two-body dynamic system in which one body is rigid and the other nonrigid. Precession of the wheel causes transient and steady-state deformations of the flexible wheel which complicate analysis.

Further study is recommended in the placement of the flywheel of the external-wheel CMG. The additional moment of inertia degrades the transient performance of the CMG, which might be corrected by more sophisticated control mechanisms.

APPENDIX A

ENERGY DENSITY OF ISOTENSOID FLYWHEELS

A proof will be given here that the energy density of a flywheel is highest if it is isotensoid. It extends from a generalization developed by J. C. Maxwell (Ref. 7) from the principle of virtual work

$$\sum_{i=1}^{n} (\sigma_{x_i} + \sigma_{y_i} + \sigma_{z_i}) V_i = \sum_{i=1}^{n} \vec{P}_i \cdot \vec{r}_i \qquad \text{(A-1)}$$

where σ_{x_i} is the stress, in one of three orthogonal directions, on the i^{th} element; σ_{y_i} and σ_{z_i} are the stresses in the other two directions; V_i is the volume; $\vec{P}_i$ is its load; and $\vec{r}_i$ is its position vector from an arbitrary origin.

The right side of the equation is the Maxwell potential, ψ_P. For a body consisting of continuous filaments it is expressed as

$$\psi_P = \int_{\ell} \vec{r} \cdot \overrightarrow{dP} .$$

The body is stressed under centrifugal loading, $\overrightarrow{dP} = m' d\ell \; \omega^2 \vec{r}_a$, where $\vec{r}_a$ is the distance from the axis. Thus

$$\psi_P = m' \; \omega^2 \int_{\ell} \vec{r} \cdot \vec{r}_a \, d\ell .$$

If the origin is located on the axis, then $\vec{r} \cdot \vec{r}_a = r_a^2$, and

$$\psi_P = m' \; \omega^2 \int_{\ell} r_a^2 \, d\ell$$

or $$\psi_p = \omega^2 I$$

where I is the moment of inertia of the body. This is twice the rotational energy of the body. Thus,

$$\sum_{i=1}^{n} \sigma_i V_i = 2E .$$

The left side of Equation (A-1) is $(\bar{\sigma}_x + \bar{\sigma}_y + \bar{\sigma}_z) V$, where $\bar{\sigma}$ is the average stress in the body, and V is the total volume. The volume may be rewritten as $V = m/\rho$, the ratio of mass to density. The energy density is then

$$\frac{E}{m} = \frac{1}{2} \frac{\bar{\sigma}_x + \bar{\sigma}_y + \bar{\sigma}_z}{\rho} .$$

This is seen to be maximum if the stresses in each direction are all equal (isotensoid) and, of course, at as high a level as possible. If the specific stress, $\lambda = \sigma/\rho g$, is now introduced, and $\bar{\sigma}$ is set equal to σ_w (maximum allowable working stress), the energy density is

$$\frac{E}{m} = \frac{f}{2} g \lambda_w \qquad (A-2)$$

where f is the number of degrees of freedom of stress action allowed. In the isotensoid filamentary flywheel, $f = 1$. In the Stodola wheel (constant biaxial stress), $f = 2$.

Additional energy is actually present in the flywheel in the form of elastic energy. This effect makes the energy greater by the factor, $(1 + \epsilon)$, where ϵ is the maximum strain. In high-stress materials, ϵ is low (around 1%). Other materials such as rubber will attain high ϵ but cannot withstand high stress levels. Thus, this effect is negligible.

APPENDIX B

ELECTROCHEMICAL ENERGY STORAGE SYSTEM

Storage batteries are of two types: primary and secondary. Primary batteries are not rechargeable, have relatively high energy density, and are used to power launch vehicles. Secondary batteries are rechargeable and hence are useful where cyclic energy requirements exist.

Four types of battery systems have been considered for space applications: nickel-cadmium, silver-zinc, silver-cadmium, and the class which uses organic solvents (Ref. 8). The nickel-cadmium battery is rechargeable, has long cycle life, and can attain moderately high energy densities. The silver-zinc battery is primary; the silver-cadmium has an energy density of about twice that of the nickel-cadmium, but its cycling characteristics at the present stage of development are poor and unpredictable. The organic-solvent type batteries promise high energy density, but are still in the research and early development stage.

The nickel-cadmium battery has been studied extensively regarding energy density, cycle life, and reliability. The results of these tests reveal a "best" way to use this battery in a mission.

The energy density of a nickel-cadmium battery (the energy obtainable per unit battery weight with a 100% discharge) is about 12 watt-hours per pound (Ref. 9). However, it has been found that battery lifetime decreases with depth of discharge, so that for reasonable battery lifetimes this energy density is not completely available. Tests have shown that at a battery temperature of 24°C the cycle life is

$$\ell = 10^{4.7-3.0\ d} \qquad \text{(B-1)}$$

where ℓ is the number of cycles to failure and d is the fractional depth of discharge.

Measurement of the discharge and charge voltages show that they are in the ratio of 0.87 to 1.0 (Ref. 8). This ratio is used as the efficiency, η , of the cell.

The total energy storage throughout the lifetime of the storage battery system per pound of battery weight is

$$\frac{E_T}{m} = \frac{E}{m} d \eta \ell \qquad \text{(B-2)}$$

Inserting an energy density of 12 watt-hr/lb, an efficiency of 0.87, and Equation (B-1) for the lifetime, the total energy is

$$\frac{E_T}{m} = 10.5 d \times 10^{(4.7-3.0 d)} \qquad \text{(B-3)}$$

The maximum of this function occurs at $d = 0.145$, so that the recoverable energy density is $E_R/m = 1.74$ watt-hr/lb, and the total energy density is $E_T/m = 2.8 \times 10^4$ watt-hr/lb. In a satellite which has an orbital period of 100 minutes, the lifetime of 1.86×10^4 cycles is equivalent to 3.5 years. Inserting a safety factor of 2.0, reducing the lifetime to 1.75 years, results in a total energy density of

$$\frac{E_T}{m} = 1.4 \times 10^4 \text{ watt-hr/lb} .$$

APPENDIX C

A STANDARD CONTROL MOMENT GYRO

A conventional CMG contains a solid rotor which has its mass concentrated at the rim for high moment of inertia. This is the best form of wheel for this purpose (see Table I). The rotor is enclosed in a sealed chamber containing low-pressure gas (Ref. 5). The CMG system consists of the rotor, a spin motor, torque motors, gimbals, the enclosure, and a power supply.

The total weight of a CMG system is primarily a function of the rotor angular momentum and of the output torque. A study relating these and finding the minimum weight of a CMG by varying system parameters has been conducted by Sperry Co. (Ref. 5). The material here is a summary of that report.

The weight of the system is the sum of the weight of the CMG and the weights added due to the volume of the system and to the power required to drive it:

$$W_T = W + A_1 P + A_2 V \qquad \text{(C-1)}$$

In the study, A_1 and A_2 were assumed 1.0 lb/watt and 1.0 lb/ft^3, respectively. The rotor angular momentum, H , and the maximum vehicle torque, T , were variables. The weight of the spin and torque motors was derived from available data concerning those motors.

The rotor was not assumed to be operating at a working stress of half ultimate, as excessive shaft speeds would be present because of the limited wheel size. Rather, the rotor size and speed were varied independently to include effects of enclosure volume and bearing and windage losses.

Results of the study were given in tabular form (data from computer runs), relating wheel angular momentum, output torque, and total CMG weight, among other things. The ratio of wheel angular momentum to total CMG weight is plotted versus wheel angular momentum for this standard CMG in Figure 18. This is the basis for comparison in evaluating the external wheel CMG.

REFERENCES

1. Kyser, A.C.: The Uniform-Stress Spinning Filamentary Disk, NASA CR-106, May 1964.

2. Fraser, A.F., Preiswerk, P.R., Benton, M.D., and Burggraf, O.R.: Axisymmetric Filamentary Structures, Astro Research Corporation Report ARC-R-274, November 1968.

3. Sperry Rand: Brushless D C Motors Applications Guide, Sperry Marine Systems Division, Charlottsville, Va., 1969.

4. ten Bosch, M.: Vorlesungen uber Machinenelemente, Springer-Verlag, 1940.

5. Davis, L. Porter: Optimization of Control Moment Gyroscope Design, Sperry Phoenix Company, 1967.

6. Crawford, R.F.: Strength, Efficiency, and Material Selection of Deployable Booms for Space Applications, Astro Research Corporation Report ARC-R-422, June 1970.

7. Maxwell, J.C.: Scientific Papers, Dover Publications, Inc., New York, 1965, Vol. II, pp 175-177.

8. Bauer, Paul: Batteries for Space Power Systems, NASA SP-172, 1968.

9. Zipkin, Morris A. and Edwards, Russell N.: Power Systems for Space Flight, Academic Press, New York, 1963, pp 211-219.

10. Hall, A.M.: Ultrahigh-Strength Steels, Machine Design, December 14, 1967.

11. Carroll-Porczynski, C.Z.: Inorganic Fibers, National Trade Press, Ltd., London 1958.

12. Hanson, Morgan P.: Glass-, Boron-, and Graphite-Filament-Wound Resin Composites and Liners for Cryogenic Pressure Vessels, NASA TN D-4412, February 1968.

TABLE I. ENERGY DENSITY (E/m), ANGULAR MOMENTUM DENSITY (H/m), AND ROTATIONAL VELOCITY (ω) OF VARIOUS TYPES OF WHEELS

Type of Wheel	E/m	H/m	ω
Isotensoid disk	$\frac{1}{2} g \lambda$	$r_0 \sqrt{\frac{1}{2} g \lambda}$	$\frac{1}{r_0} \sqrt{2g \lambda}$
Isotensoid spindle	$\frac{1}{8} g \lambda$		
Standard disk	$\frac{2}{3+\nu} g \lambda$	$r_0 \sqrt{\frac{2}{3+\nu} g \lambda}$	$\frac{1}{r_0} \sqrt{\frac{8}{3+\nu} g \lambda}$
Standard hoop	$\frac{1}{2} g \lambda$	$r_0 \sqrt{g \lambda}$	$\frac{1}{r_0} \sqrt{g \lambda}$
Standard rod	$\frac{1}{3} g \lambda$	$\ell_0 \sqrt{\frac{2}{9} g \lambda}$	$\frac{1}{\ell_0} \sqrt{2g \lambda}$
Stodola wheel	$g \lambda$	$r_0 \sqrt{\frac{1}{2} g \lambda}$	$\frac{1}{r_0} \sqrt{5g \lambda}$

$\lambda = \frac{\sigma}{\gamma}$ = specific stress

ν = Poisson's ratio

r_0 = radius of wheel

ℓ_0 = length of rod (spinning about one end)

TABLE II. SPECIFIC WORKING STRESS OF VARIOUS MATERIALS

Material	Ultimate Stress	Density	Specific Working Stress (λ_w)	Ref.
Steel (18% Ni Maraging)	345 000 lb/in.^{2}	0.283 lb/in.^{3}	600 000 in.	10
Steel (A-572 Grade 65)	80 000 lb/in.^{2}	0.283 lb/in.^{3}	141 600 in.	10
Dacron tape	145 lb	8.8×10^{-5} lb/in.	800 000 in.	
Glass yarn	0.6 lb	3.1×10^{-7} lb/in.	1 000 000 in.	11
Glass filament	650 000 lb/in.^{2}	0.09 lb/in.^{3}	3 600 000 in.	12
Boron filament	500 000 lb/in.^{2}	0.09 lb/in.^{3}	2 800 000 in.	12
Graphite filament	200 000 lb/in.^{2}	0.054 lb/in.^{3}	1 800 000 in.	12
7 x 7 SS cable (1/16 in.)	900 lb	6.25×10^{-4} lb/in.	720 000 in.	

Note: Specific working stress = $\frac{0.5 \text{ (ultimate stress)}}{\text{density}}$

TABLE III. COMPARISON OF INTERNAL AND EXTERNAL CONTROL-MOMENT GYRO SYSTEMS

		Internal Wheel	External Wheel	
			Small	Large
(H)	Angular momentum (ft-lb-sec)	2000	2000	10 000
(T)	Max. gimbal torque (ft-lb)	667	667	667
(r_0)	Rotor radius (ft)	1.17	6.53	11.16
	Rotor speed (rpm)	7857	2876	1681
(W_{disk})	Rotor weight	71.1	10.04	29.36
(W_G)	Gimbal weight	55.4	10.04	29.36
(W_B)	Boom weight	--	11.96	20.45
(W_{TM})	Torque weight	65	25.12	1.45
(W_{SM})	Spin motor weight	3.1	2.33	1.99
(W_{PS})	Power system weight	77	46.47	22.04
(W_{vol})	Volume weight	34	9	45
	Miscellaneous weight	40	--	--
(W_T)	Total weight	345	115	149
(H/W_T)	Specific angular momentum	5.8	18.1	67

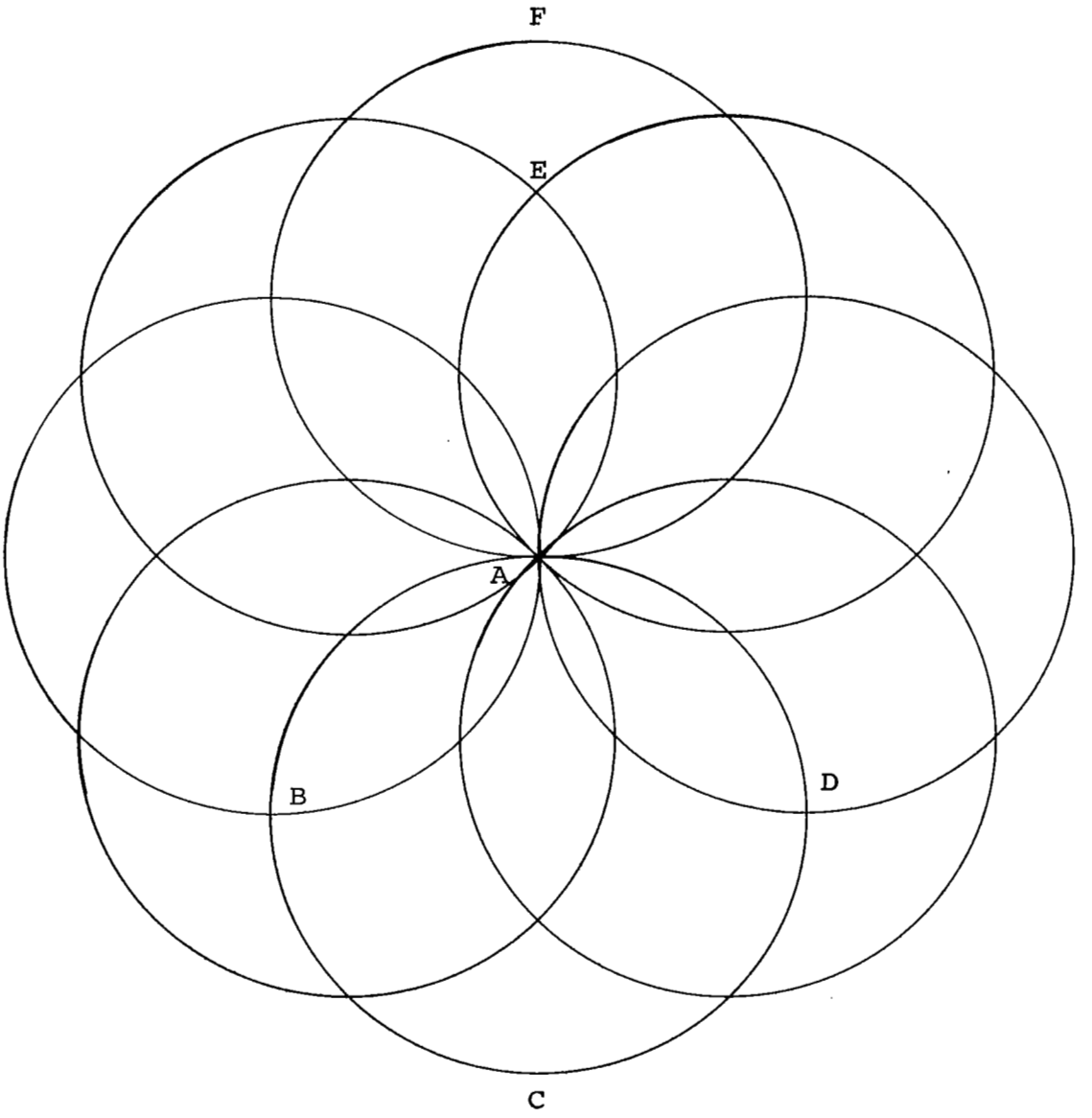

Figure 1. Disk Isotensoid

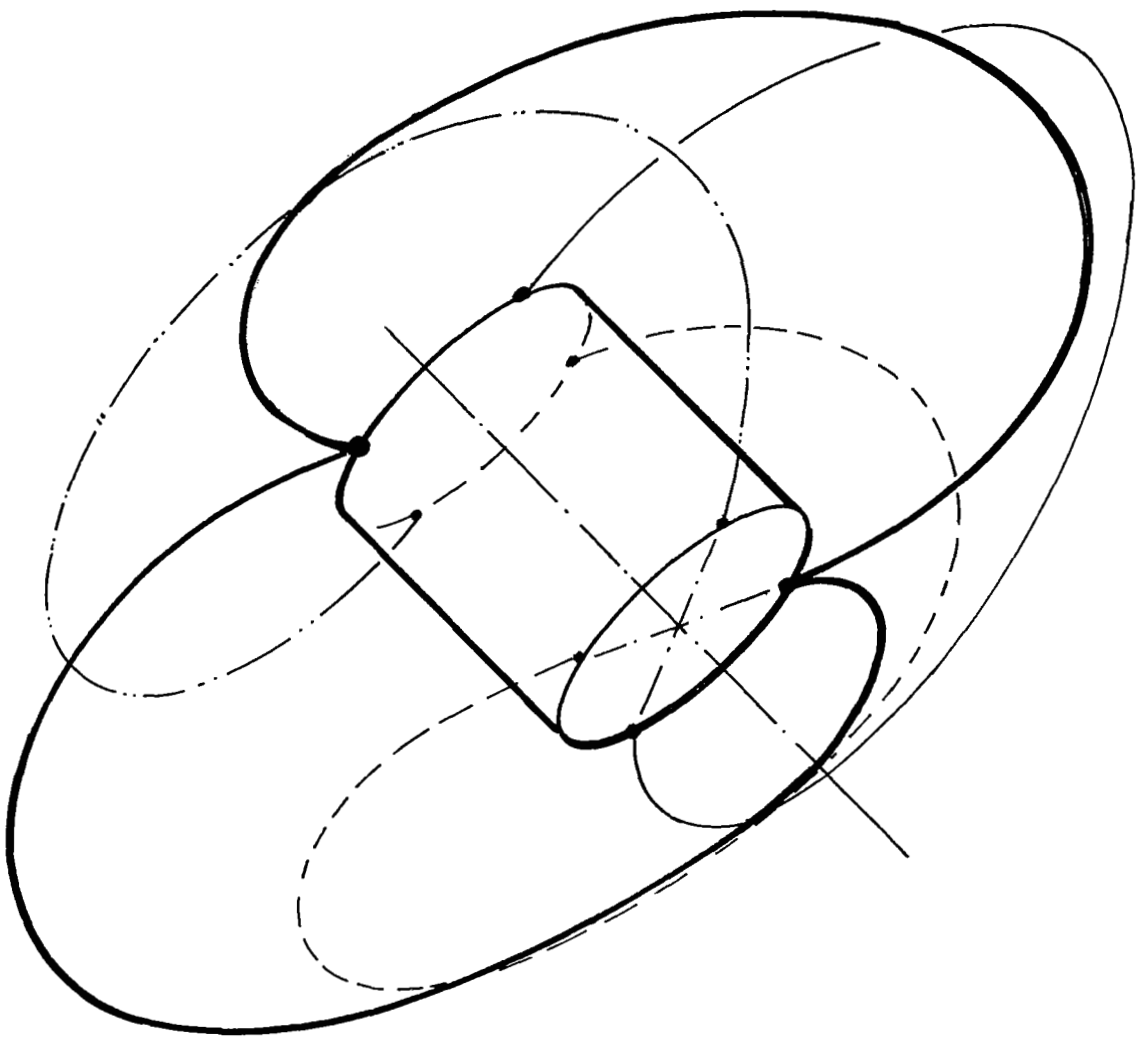

Figure 2. General Isotensoid Shape

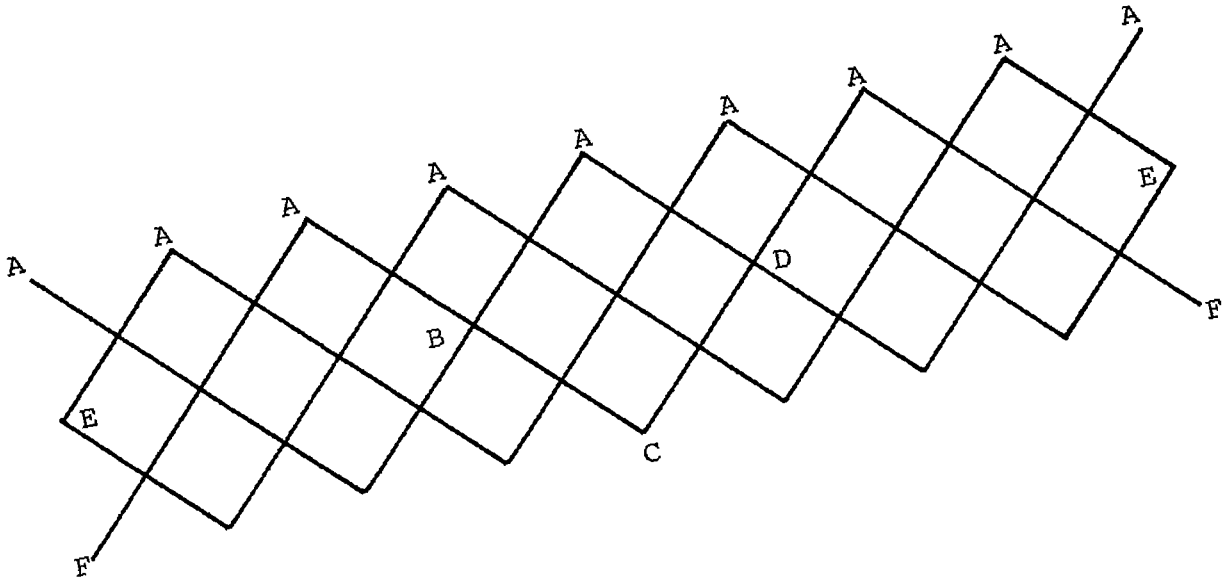

Figure 3. Map of Isotensoid (Compare to Figure 1)

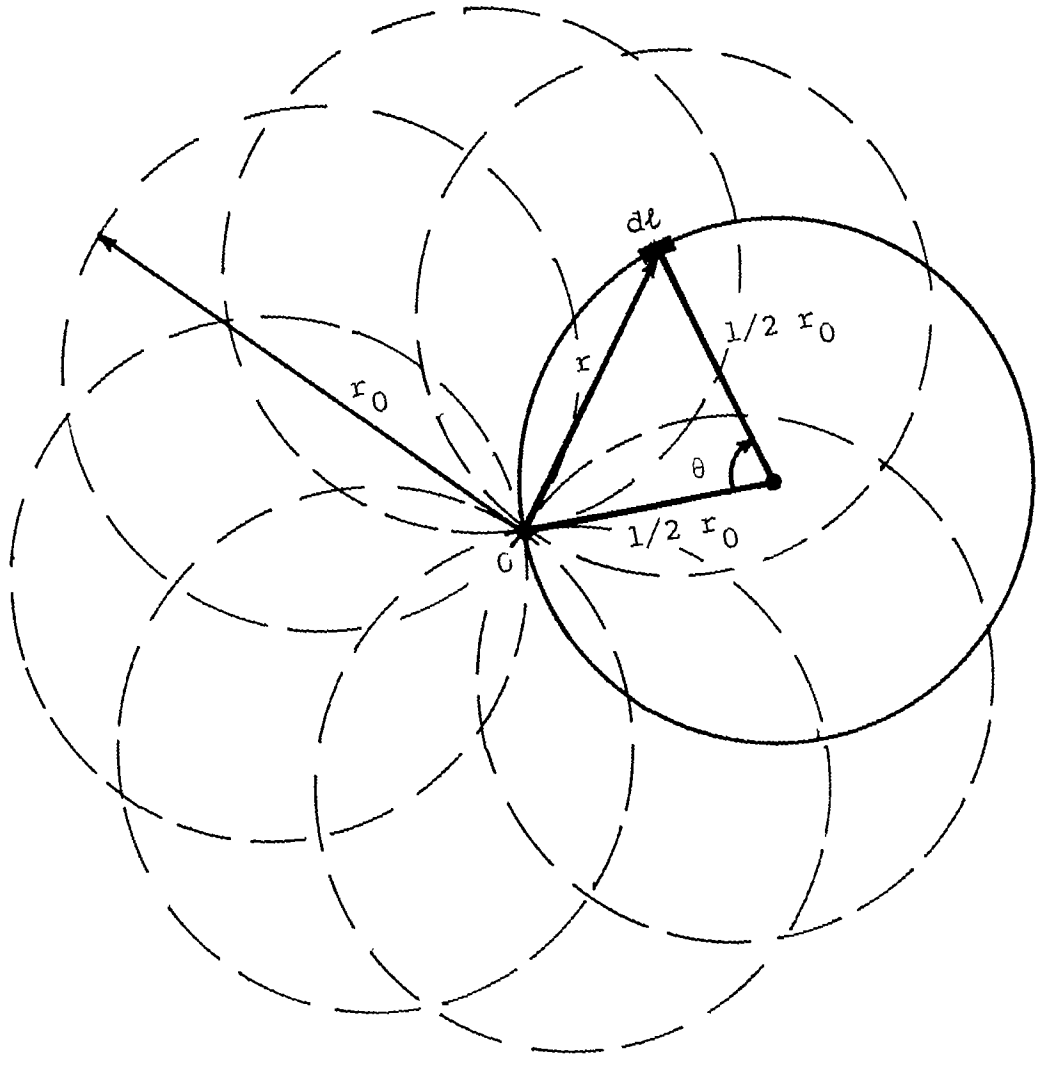

Figure 4. Determining the Radius of Gyration of the Isotensoid Disk

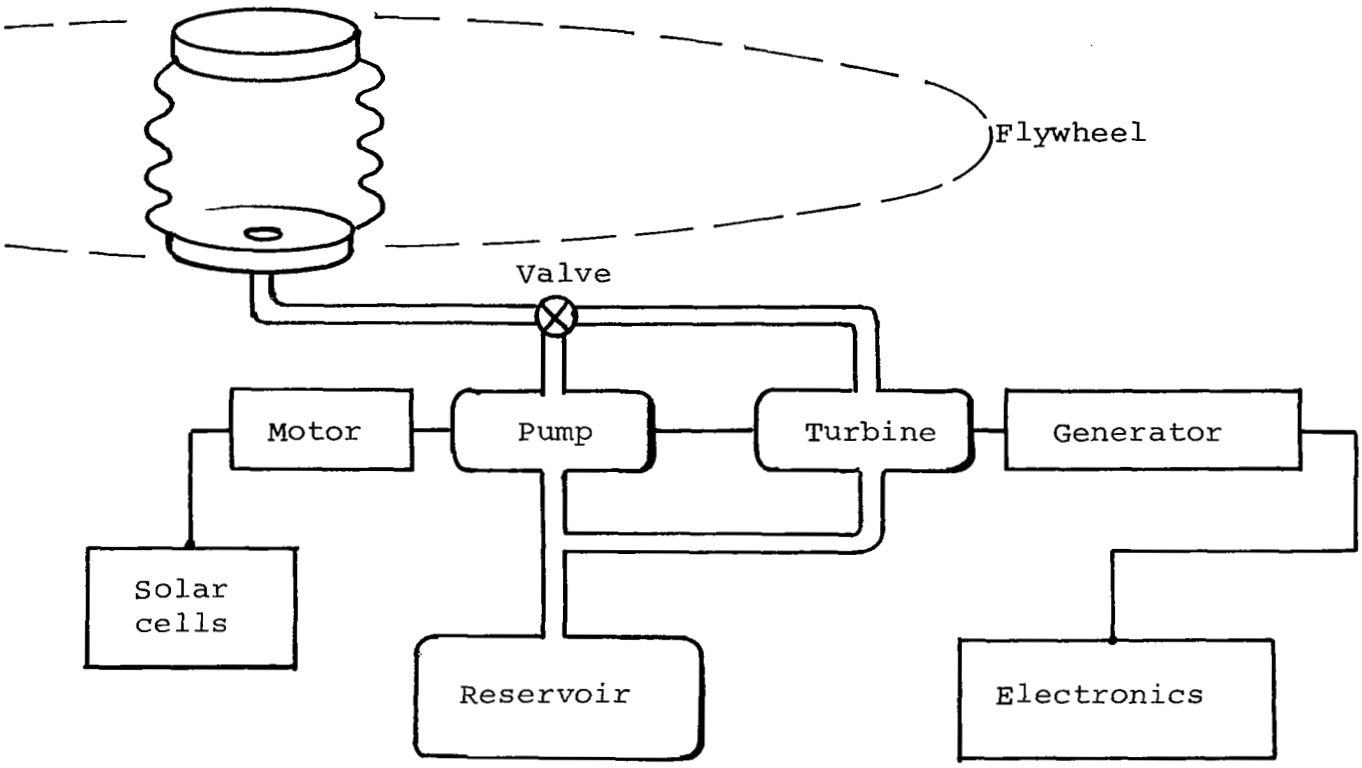

Figure 5. Possible Configuration for Energy Transfer Using Double-Hub Flywheel

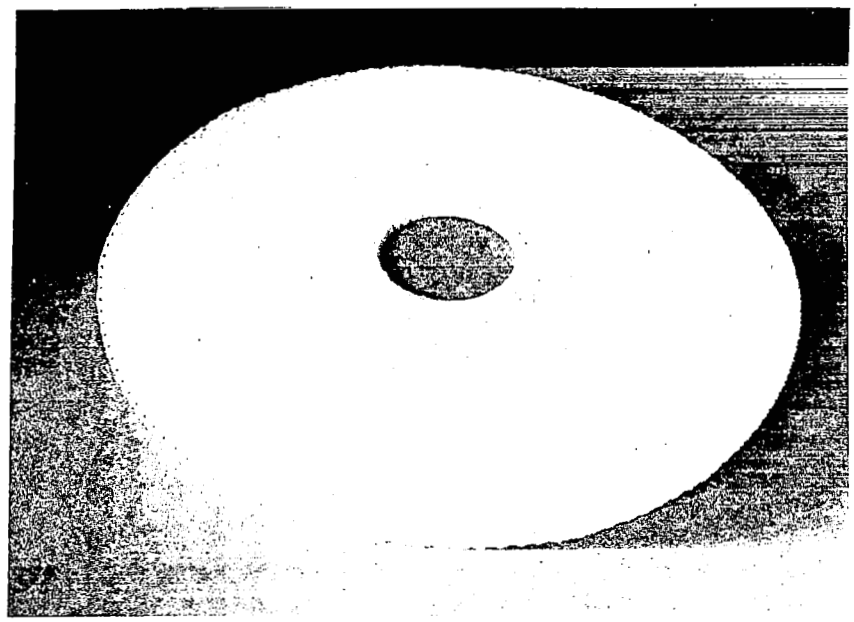

Figure 6 Woven Dacron Isotensoid Disk

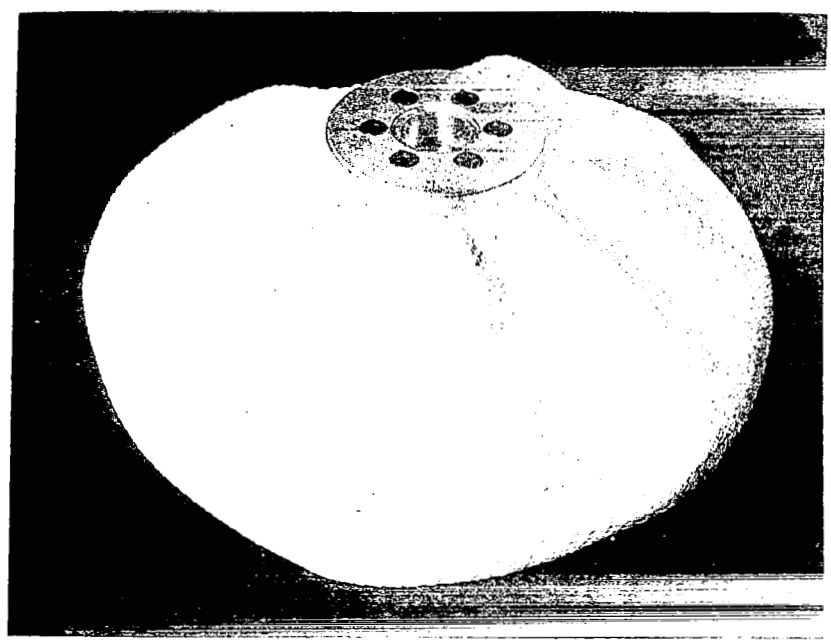

Figure 7 Woven Dacron Isotensoid Spindle

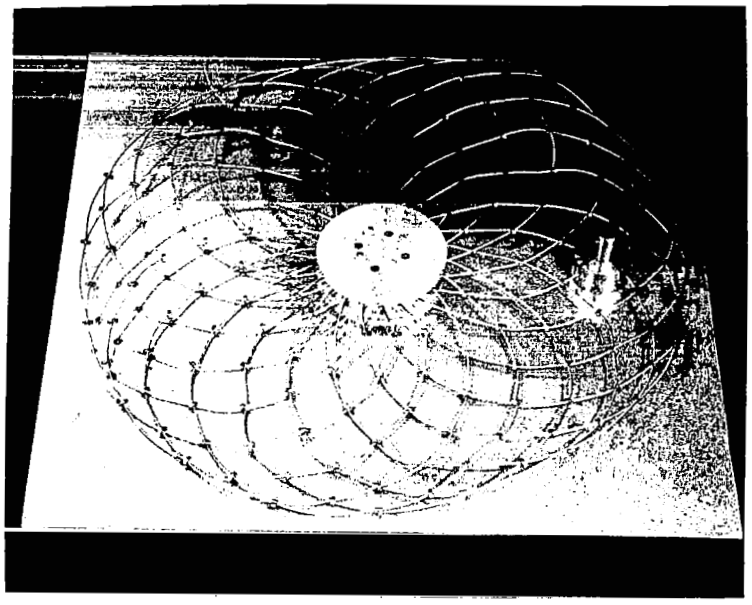

Figure 8 Construction of Stainless Steel Cable Isotensoid Flywheel

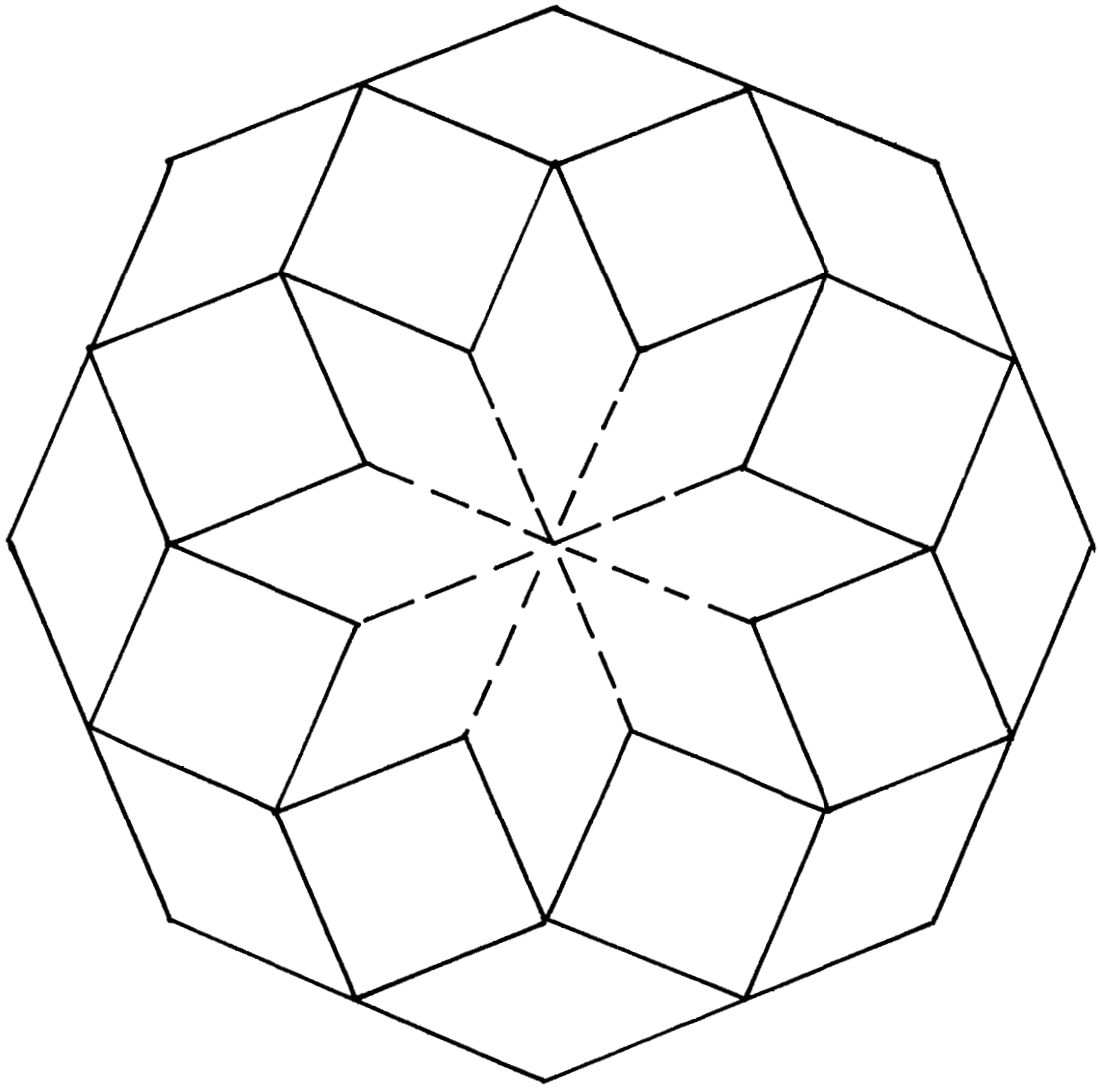

Figure 9. Semisolid Isotensoid Flywheel

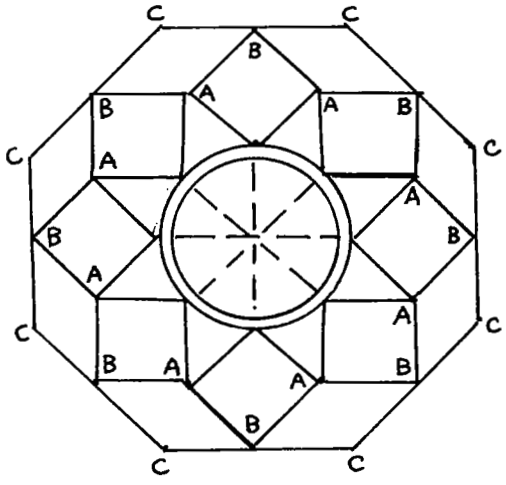

a) Move points A up to hub

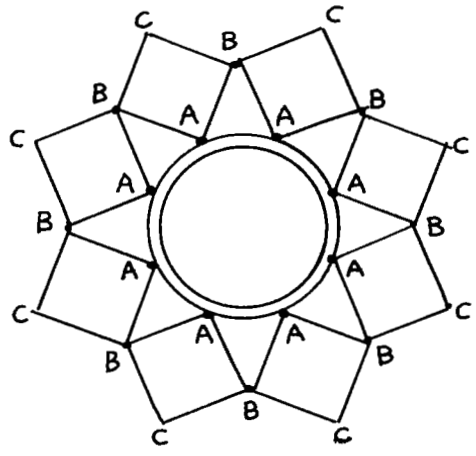

b) Move points B down to hub

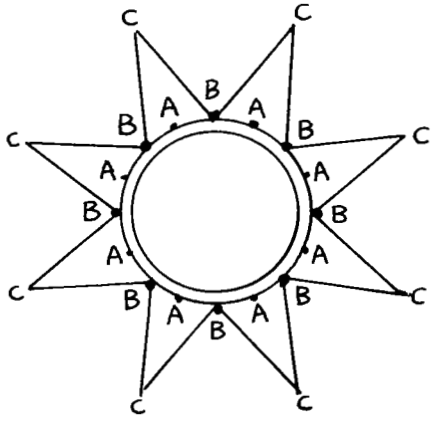

c) Move points C up to hub

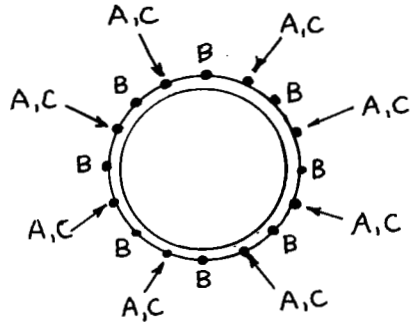

d) Packaged

Figure 10. Packaging Scheme of Semisolid Isotensoid Flywheel

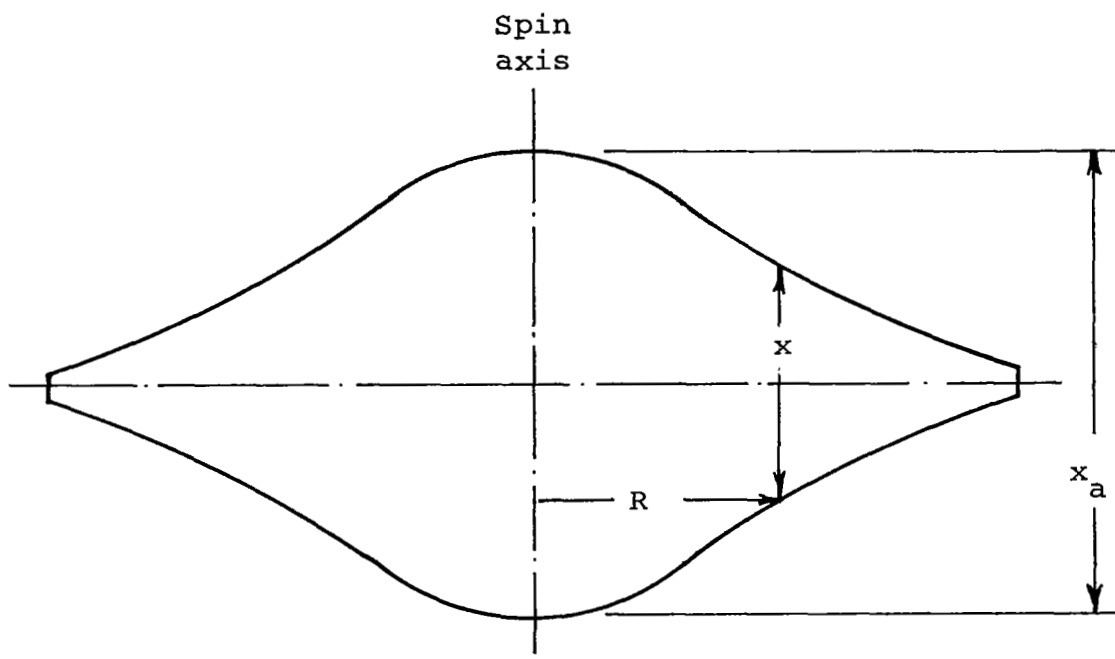

Figure 11. Constant Biaxial Stress (Stodola) Wheel:
$x = x_a e^{-\frac{1}{2}\Gamma R^2}$ with $\Gamma = 5.0$

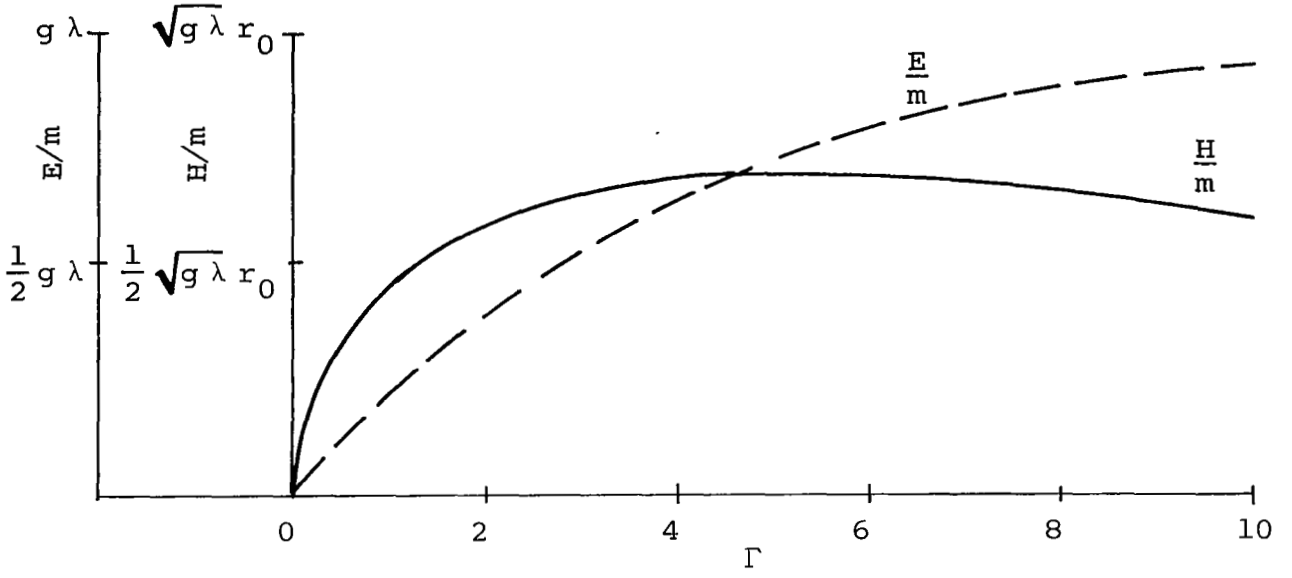

Figure 12. Energy and Momentum Densities (E/m and H/m) of Stodola Wheel as a Function of Γ

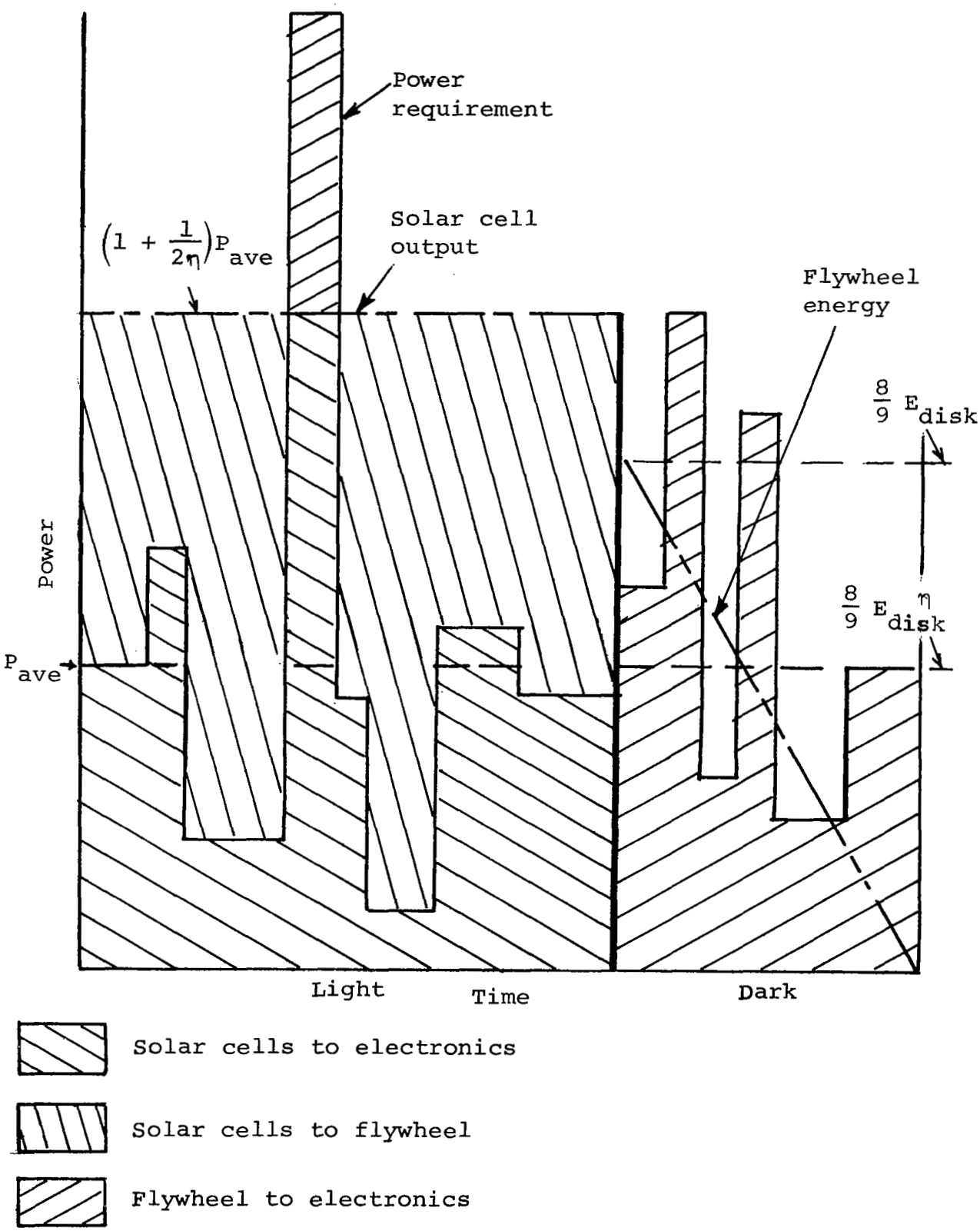

Figure 13. Power Cycle During Single Orbit

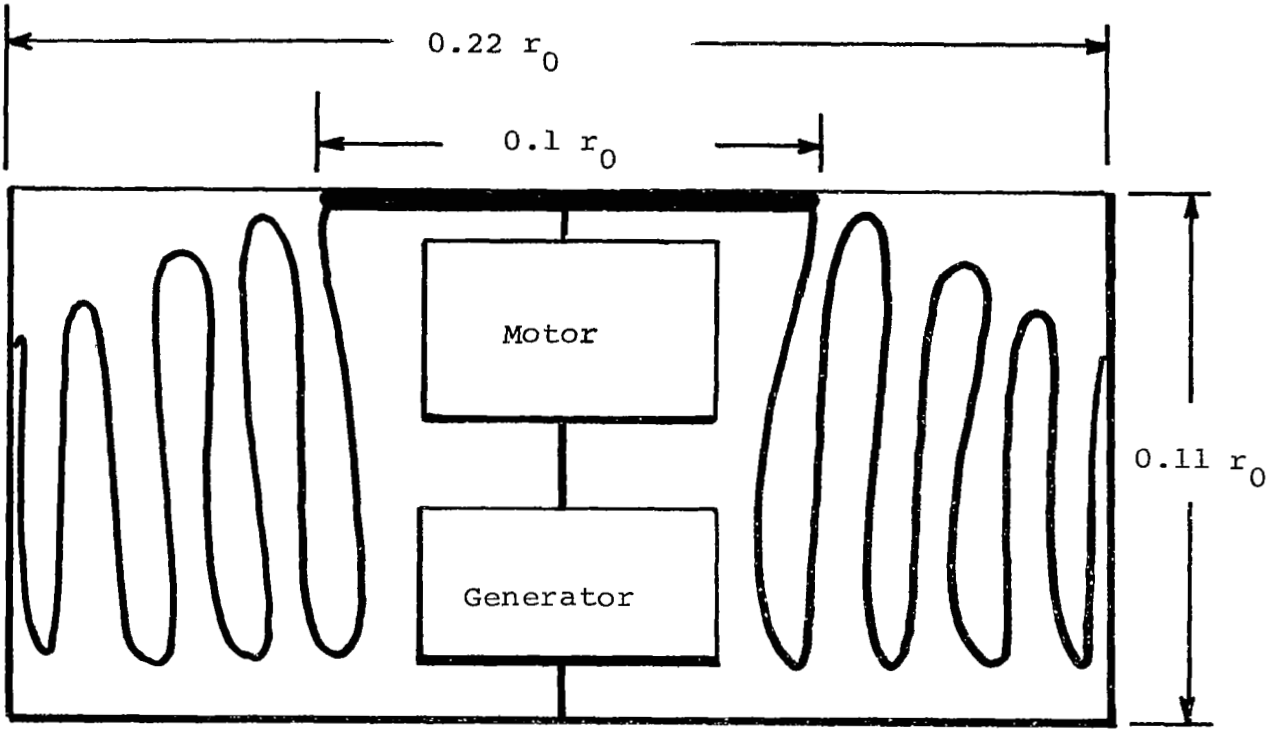

Figure 14. Package Design of Isotensoid Disk Flywheel Energy Storage System

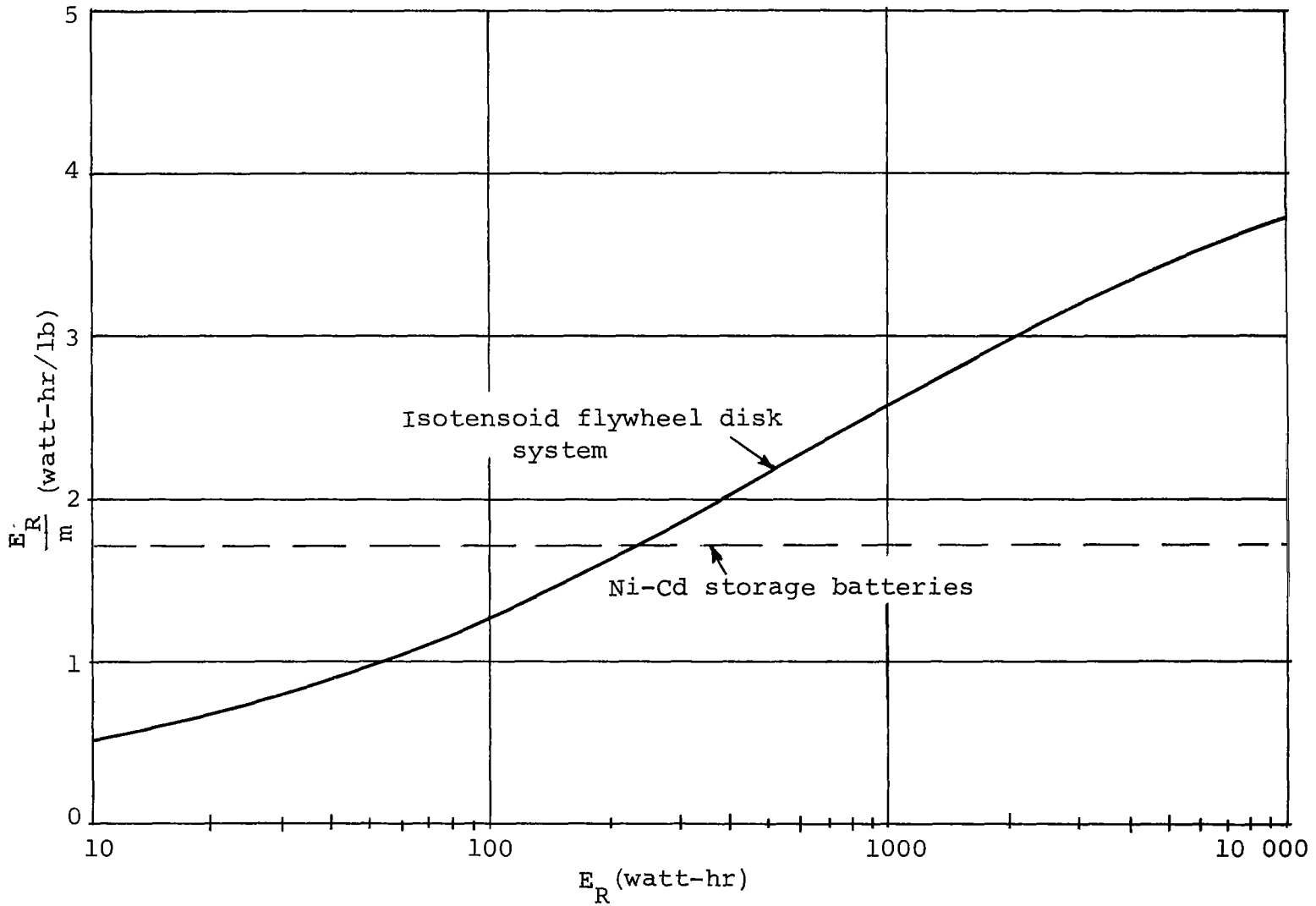

Figure 15. Energy Density of Isotensoid Flywheel Energy Storage System

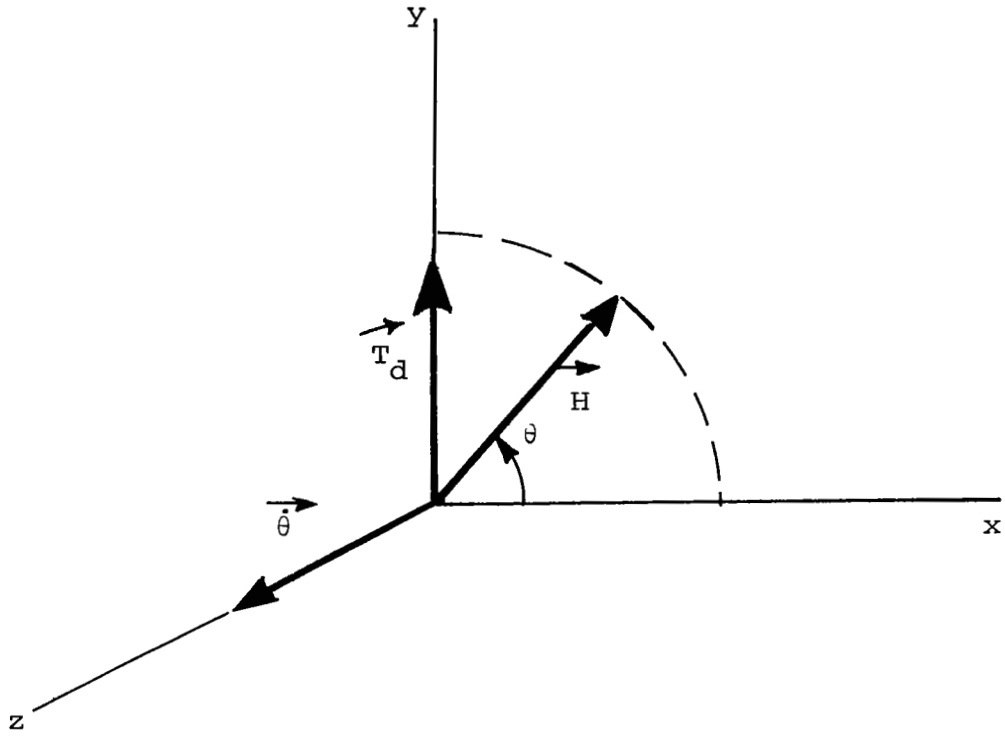

Figure 16. Gyroscopic Action

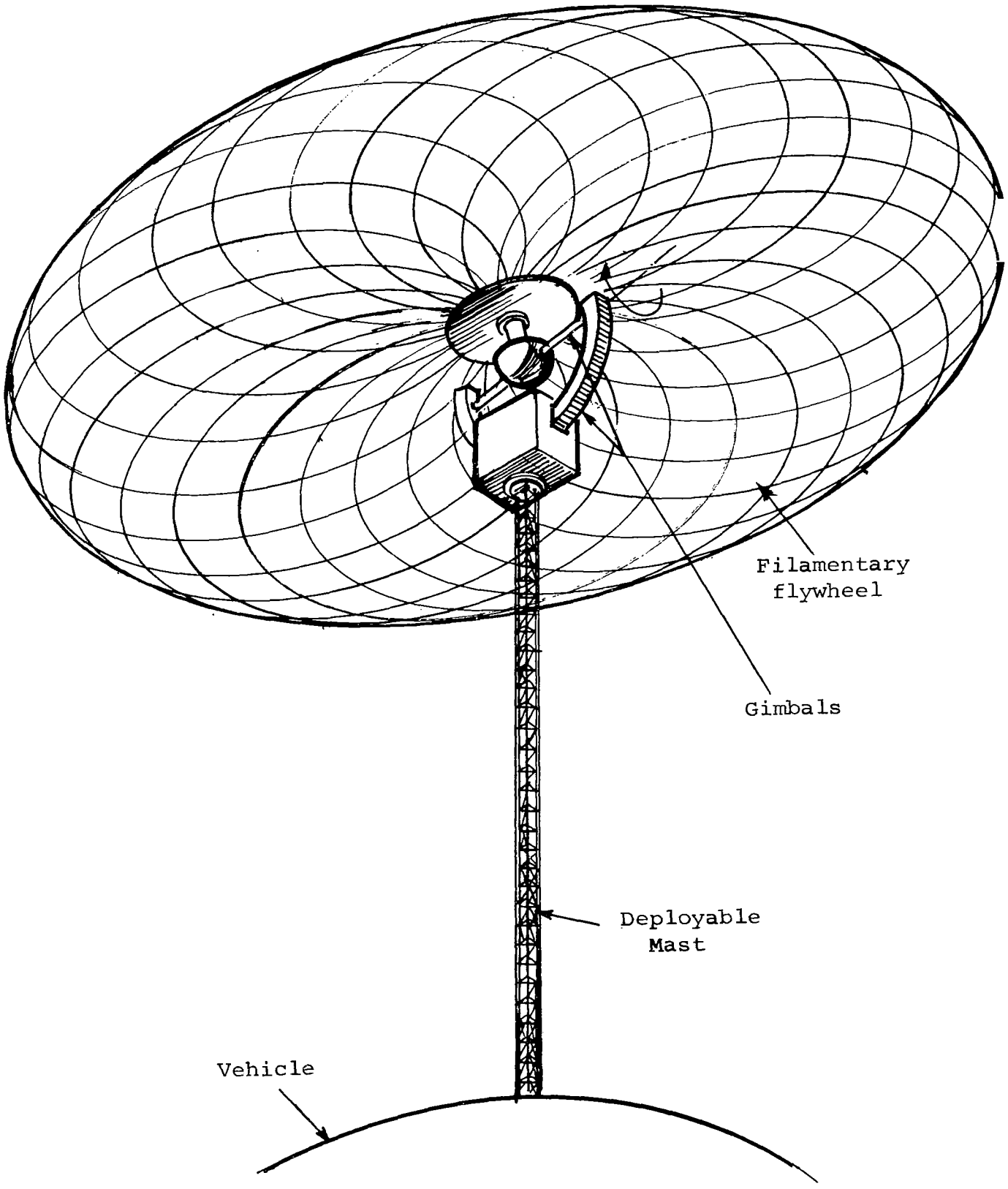

Figure 17. External Wheel Control Moment Gyro

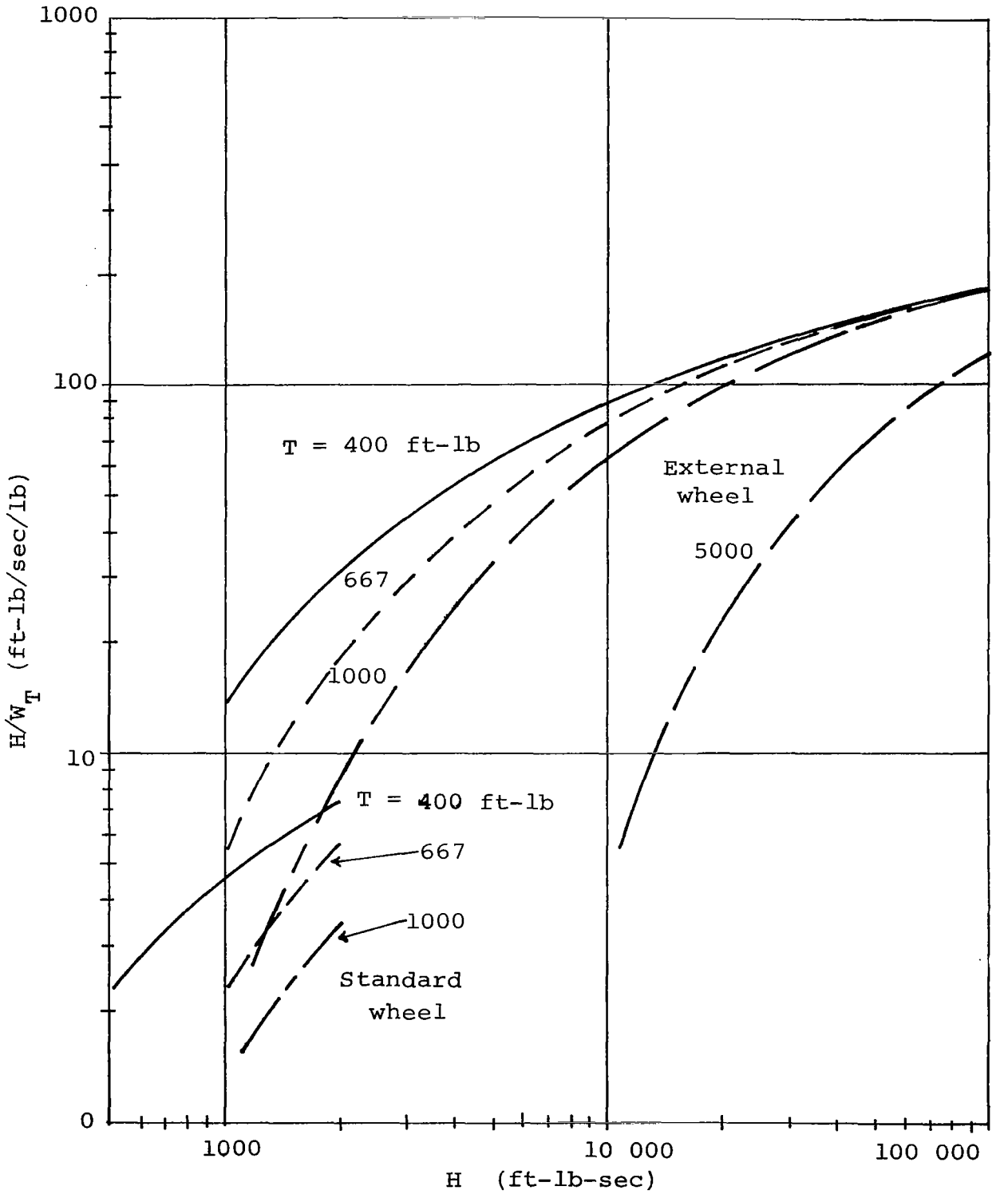

Figure 18. Comparison of External Wheel to Standard CMG: Flywheel Angular Momentum per pound CMG (H/W_T) versus Flywheel Angular Momentum (H) versus Output Torque (T)

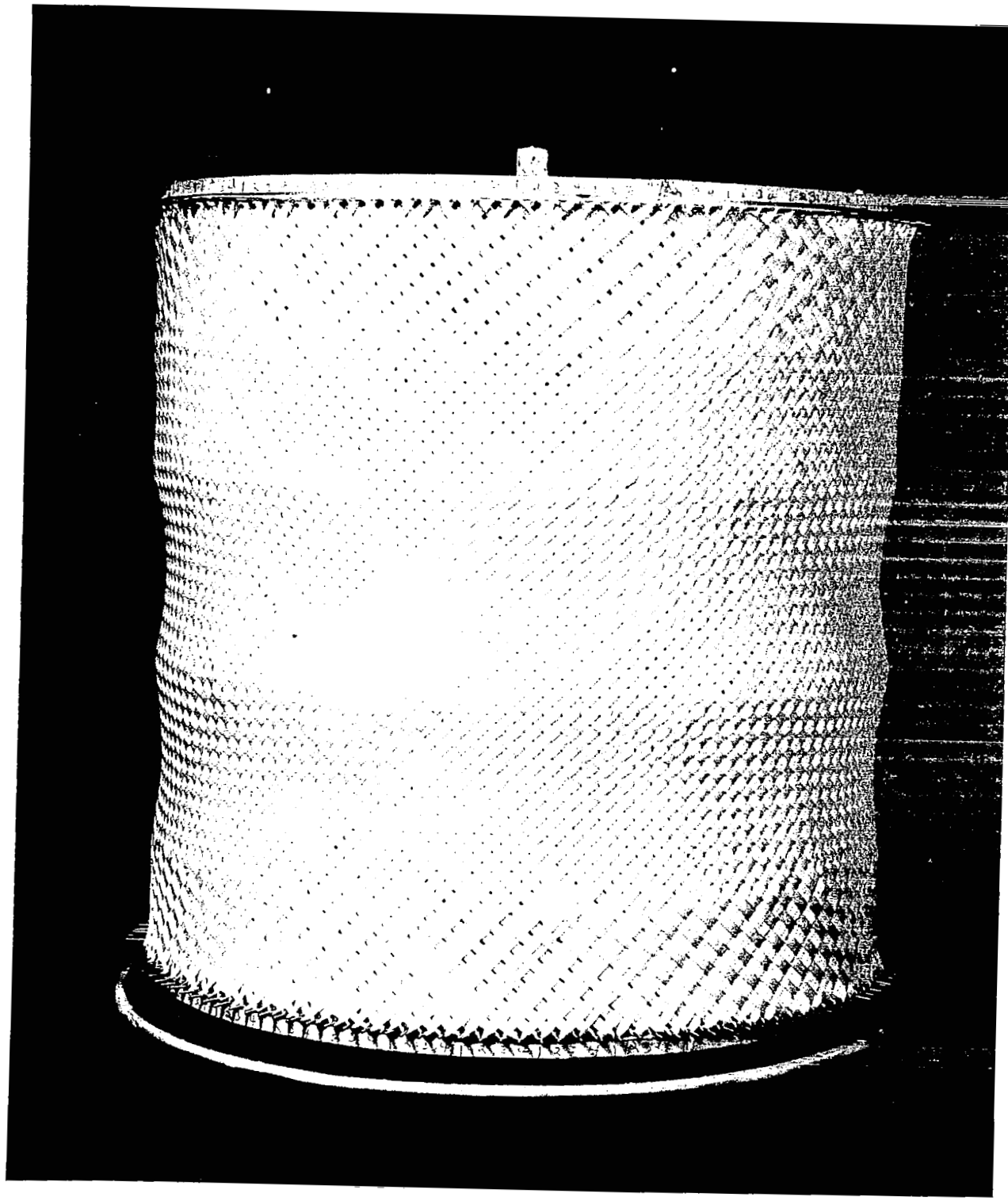

Figure 19 Woven Dacron Flywheel on Construction Drum

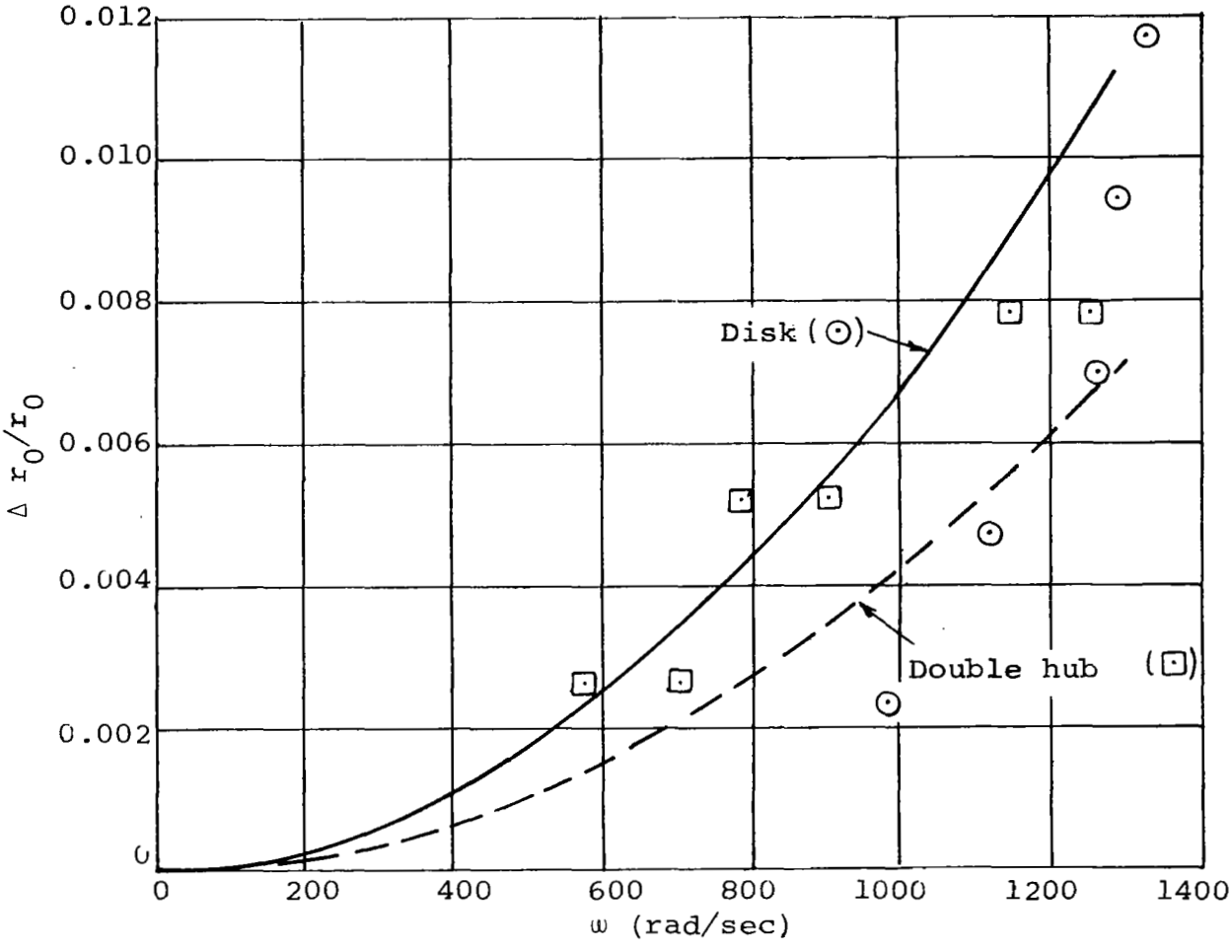

Figure 20. Fiber Elongation Test Results: Fractional Change in Wheel Radius versus Spin Speed for Disk and Double-Hub Isotensoid
(Theoretical Curves and Experimental Points)